CONFIDENTIAL









# RESEARCH MEMORANDUM

## FREE-FLIGHT AERODYNAMIC-HEATING DATA TO A MACH NUMBER OF 15.5 ON A BLUNTED CONICAL NOSE WITH A TOTAL ANGLE OF 29°

By William M. Bland, Jr., Charles B. Rumsey,
Dorothy B. Lee, and Ronald Kolenkiewicz

Langley Aeronautical Laboratory
Langley Field, Va.



NATIONAL ADVISORY COMMITTEE
FOR AERONAUTICS

WASHINGTON

August 1, 1957

CONFIDENTIAL

NATIONAL ADVISORY COMMITTEE FOR AERONAUTICS

RESEARCH MEMORANDUM

# FREE-FLIGHT AERODYNAMIC-HEATING DATA TO A MACH NUMBER OF 15.5 ON A BLUNTED CONICAL NOSE WITH A TOTAL ANGLE OF 29°

By William M. Bland, Jr., Charles B. Rumsey, Dorothy B. Lee, and Ronald Kolenkiewicz

## SUMMARY

A five-stage rocket-propelled model has been flown to a Mach number of 15.5 and a corresponding free-stream Reynolds number per foot of $1.88 \times 10^6$ at an altitude of 98,200 feet. Temperatures were measured at six stations along the inside surface of a blunted conical nose with a total angle of 29° which was fabricated from Inconel and was smoothly polished. The maximum measured temperature was 2,470° F.

Maximum heat flux was about 1,000 Btu/(sec)(sq ft) at all temperature measuring stations except at the most forward and at the next-to-last stations which had 700 and 1,650 Btu/(sec)(sq ft), respectively. The experimental heat flux at the first temperature measuring station agreed well with theoretical values obtained for laminar, equilibrium, dissociated flow, but the experimental values became increasingly greater than the theoretical laminar-flow values at the more rearward temperature measuring stations.

When compared with Stanton numbers obtained from turbulent- and laminar-flow theories by applying perfect-gas relations, the experimental Stanton numbers, likewise obtained by applying perfect-gas relations, indicated that the flow was laminar at the two forward temperature measuring stations except at the second station near the end of the test. Also, the flow at the other stations followed a pattern that indicated the presence of laminar flow that was interrupted by a burst of turbulence, of transitional flow beginning at a free-stream Mach number and Reynolds number per foot of $11.0 \times 10^6$ and $1.4 \times 10^6$, respectively, and of turbulent flow near the end of the test.

Extremely high Stanton numbers obtained at the end of the test when the nose skin was close to the melting temperature are believed to have been caused by either nose distortion or surface disfiguration or both.

## INTRODUCTION

The problems of aerodynamic heating and boundary-layer transition on bodies moving at supersonic and hypersonic speeds are currently being investigated by the Langley Pilotless Aircraft Research Division by means of techniques that utilize rocket-propelled models in free flight. Results of some recent flight tests which utilized four-stage-rocket systems, first proved feasible by the test reported in reference 1, are presented in reference 2 to a Mach number of 10.4 and in reference 3 to a Mach number of 9.89. As a result of the pressing need to obtain aerodynamic heat-transfer data at even higher Mach numbers, a five-stage-rocket system has recently been developed. The first results obtained with the five-stage-rocket system are reported in reference 4 to a Mach number of 13.9.

Another flight test utilizing the five-stage-rocket system has been made to obtain aerodynamic heat-transfer data on a smoothly polished blunted conical nose with a total angle of 29°. These data are presented herein for free-stream Mach numbers between 2.0 and 15.5 corresponding to free-stream Reynolds numbers per foot between $0.25 \times 10^6$ and $1.88 \times 10^6$. The flight test was conducted at the Langley Pilotless Aircraft Research Station at Wallops Island, Va., on March 22, 1957. The fourth-stage rocket motor (JATO, 1.52-KS-33,550,XM19 "Recruit") used in the present investigation was made available by the U. S. Air Force.

## SYMBOLS

| | |
|---|---|
| C. G. | center of gravity |
| $c_f$ | local skin-friction coefficient |
| $c_p$ | specific heat of air at constant pressure, Btu/(lb)(°F) |
| g | gravitational constant, 32.2 ft/sec$^2$ |
| h | local aerodynamic heat-transfer coefficient, Btu/(sec)(sq ft)(°F) |
| M | Mach number |
| $N_{St}$ | Stanton number, $\frac{h}{gc_p\rho V}$ |
| $N_{Pr}$ | Prandtl number |
| q | heat flux, Btu/(sec)(sq ft) |

| | |
|---|---|
| R | Reynolds number, $\frac{\rho V x}{\mu}$ |
| T | temperature, $^{\circ}F$ except as noted |
| t | time, sec |
| V | velocity, ft/sec |
| x | distance along nose surface from stagnation point, ft |
| $\epsilon$ | emissivity |
| $C_p$ | pressure coefficient |
| $C_{p,t}$ | total-pressure coefficient behind normal shock |
| $\theta$ | semivertex angle of cone tangent to hemisphere, deg |
| $\rho$ | density of air, slugs/cu ft |
| $\mu$ | absolute viscosity of air, slugs/ft-sec |

Subscripts:

| | |
|---|---|
| aw | adiabatic wall |
| $\infty$ | undisturbed free stream ahead of model |
| t | stagnation |
| $l$ | local condition just outside boundary layer |
| w | wall |

## MODEL, INSTRUMENTATION, AND TEST TECHNIQUE

### Model

The model, as shown in figure 1, was a body of revolution 67.36 inches long having a blunted conical nose with a total angle of 29°, a stepped cylindrical midsection, and a conical frustum at the tail with a total angle of 20°.

The conical sides and attached short cylindrical section of the nose were fabricated from 0.05-inch-thick Inconel that was closed at the front

end by a 1/4-inch-thick disk of Inconel. A layer of nickel was added to the outside of the Inconel disk and was then carefully machined to a 5/8-inch-radius hemisphere, thus making the ratio of the nose radius to the base radius equal to 0.25.

Installed inside the nose was a radiation shield, spaced 0.2 inch from the inside surface of the skin, to protect instruments and equipment from the high skin temperatures expected on the nose. This shield, which was fabricated from 0.05-inch-thick Inconel, was insulated from the external skin by a 1/16-inch-thick asbestos spacer at the front and by a ring of 1/8-inch-thick insulating material at the rear of the short cylindrical section. These and other details of the nose are shown in figure 2.

The forward cylindrical midsection, of double-wall construction, housed most of the telemetering equipment. A short conical frustum having a total angle of 20° joined the forward cylindrical section with the larger rear section which contained the fifth-stage rocket motor.

Stabilization of the model was achieved by a conical frustum having a total angle of 20° attached to the rear of the model. In addition to stabilizing the model, this frustum also served as an extension to the rocket-motor nozzle.

All external surfaces of the model were polished, but particular attention was given to polishing the hemispherical nose tip and the nose cone since all the thermocouples installed in the model measured temperatures on the cone. As a result of careful polishing, measurements indicated a surface roughness of 3 microinches on the hemispherical nose tip, 5 microinches on the nose cone, and no more than 9 microinches on the cylindrical portion of the nose section. Measurements were made with a fringe-type interference microscope.

Photographs of the blunted nose cone and of the complete model are presented in figures 3 and 4, respectively.

## Instrumentation

Measurements by six thermocouples and five accelerometers were transmitted from the model during the flight by means of a six-channel telemeter. The thermocouples, made of no. 30 gage chromel-alumel wire, were spot-welded to the inner surface of the Inconel skin at the stations indicated in figure 2. Distances from the stagnation point to each thermocouple and skin thicknesses measured at each thermocouple station are also presented in figure 2.

Three constant voltages and outputs of each of the six thermocouples were commutated and transmitted on one telemeter channel at rates of four times per second and eight times per second, respectively. The constant voltages were chosen to be equivalent to the lowest, middle, and highest temperatures anticipated in order to serve as an inflight check calibration of the thermocouple-telemetering system.

Each of the remaining five telemeter channels was used to transmit continuous measurements of one of five accelerometers: three measured longitudinal accelerations, one measured transverse acceleration, and one measured normal acceleration. These accelerometers were calibrated in gravitational units for the following ranges in which the positive values indicate thrust or positive force acting on the model:

| | |
|---|---|
| Two longitudinal accelerometers | -25 to 140 |
| One longitudinal accelerometer | -4 to 1 |
| Transverse and normal accelerometers | -25 to 25 |

Other instrumentation consisted of ground-based radar units for measuring model velocity and for obtaining the position of the model in space. The velocity measuring unit tracked the model until the range became too great at about 24 seconds. For times thereafter, velocity was obtained by integrating the longitudinal-accelerometer measurements. Atmospheric conditions and wind data were measured to an altitude of about 103,600 feet by a rawinsonde carried aloft by a balloon which was tracked by a modified radar unit. These measurements were made at the altitude of the high-speed portion of the flight within approximately 15 minutes of the flight.

## Test Technique

The desired performance was attained by using a five-stage propulsion system consisting of solid-fuel rocket motors. The model, which contained one of the rocket motors, and the four booster stages are shown in figure 5 as they appeared on the launcher. Characteristics of the rocket motors are presented in table I.

The model-booster combination was launched at an angle of 74° above the horizontal. The first two stages, in delayed sequence, were used to propel the remaining stages along a trajectory that reached a peak altitude of about 98,200 feet. Near the summit of the trajectory the remaining three propulsion stages were used in rapid sequence to accelerate the model to its maximum velocity along a flight path inclined slightly above the horizontal.

## ACCURACY

The measured temperatures are believed to be accurate within ±1 percent of the full-scale range of the thermocouples. Therefore, any skin-temperature measurement is believed to be accurate within ±24° F.

The possible error in Mach number at the time of third-stage ignition is estimated to be ±0.10. Because of the method of data reduction used, the possible error in Mach number accumulated during the acceleration of the last three stages and amounted to about ±0.15. Therefore, the Mach number at the end of the test is believed to be accurate within ±0.25.

## RESULTS AND DISCUSSION

### Flight Test

The trajectory followed by the model until the time the telemeter signal ceased, near burnout of the fifth-stage rocket motor, is presented in figure 6. Times of significant events are indicated on the trajectory. Performance of the model and atmospheric conditions encountered during the flight test are presented against time from take-off in figures 7, 8, and 9. A maximum Mach number of 15.5 was attained at an altitude of 98,200 feet when the telemeter signal ceased, 92.3 seconds after take-off. At this time, the rocket motor was still providing thrust to accelerate the model at approximately 590 $ft/sec^2$.

### Skin Temperatures

Time histories of the temperatures measured on the inside surface of the skin at each of the six temperature measuring stations are presented in figure 10 for the time interval between 85 and 92.3 seconds. The measured temperature increased during this interval, particularly near the end of the flight test when the Mach number was approaching its maximum value. Maximum measured inside skin temperatures, beginning with the measurement at thermocouple station 1 and proceeding rearward in order, were 1,757° F, 2,025° F, 1,975° F, 2,130° F, 2,470° F, and 1,760° F. Since the thermocouple outputs were commutated, in order from station 1, the temperatures were not measured simultaneously; this explains the large difference in maximum temperatures between station 5, which was the last station measured, and station 6. The rate of change of temperature at station 5 at 92.2 seconds was 5,293° F per second. An unpublished computational method was used to calculate the temperature difference through the Inconel skin so that the outside skin temperatures, presented

in figure 11, could be determined. Temperature differences through the skin of several hundred degrees were calculated near the end of the test. The resulting outside skin temperatures corresponding to the maximum temperatures measured on the inside surface are 2,150° F, 2,439° F, 2,431° F, greater than 2,500° F*, greater than 2,500° F*, and 2,117° F, respectively. The magnitude of these maximum temperatures indicates that the melting temperature of Inconel, 2,500° F, was reached on the surface and was closely approached on the inside of the skin at the end of the flight test.

## Heat-Transfer Data

Time histories of the net heat flux to the nose skin are presented in figure 12. Net heat flux is the gross (total) aerodynamic heat transferred to the skin minus the heat lost by radiation. Maximum values of the order of 1,000 Btu/(sec)(sq ft) were obtained at most stations except for station 1 which had a maximum heat flux of 700 Btu/(sec)(sq ft) and for station 5 which had a maximum heat flux of about 1,650 Btu/(sec)(sq ft). These values of heat flux were calculated by using the time rate of change of the average skin temperature (average between measured inside temperatures and the outside skin temperatures). Values of the heat flux at station 1 obtained by using the time rate of change of the temperature of the inside wall are also presented (fig. 12(g)) to illustrate by comparison with the values in figure 12(a) the small differences in heat flux involved, which were less than 10 percent of the instantaneous heat flux.

Since these net heat-flux values differ from the gross heat-flux values because of external- and internal-radiation heat losses by only about 3 percent, they were considered satisfactory for comparison with theoretical values. Therefore, the net heat flux at each temperature measuring station for a portion of the flight-test period is compared in figure 13 with theoretical values that include dissociation effects. Theoretical stagnation-point heat-flux values were obtained by assuming laminar flow and dissociation equilibrium behind a normal shock (ref. 5) for a Lewis number of 1.0. Material from reference 6 was used to modify the stagnation-point values for different positions along the cone. Agreement between experimental and theoretical laminar-flow values was good at the temperature measuring station nearest the nose. At the more rearward thermocouple stations the experimental values became progressively higher than the theoretical values for laminar flow.

The experimental heat-flux values were further reduced to aerodynamic heat-transfer coefficients by the heat-balance relation in reference 2

*Since the calculations do not account for changes in state, indicated outside skin temperatures greater than the melting temperature of Inconel are presented as the melting temperature.

which has provisions for external- and internal-radiation heat losses. The variation of emissivity of Inconel with temperature (ref. 7) is presented in figure 14. The emissivity of unoxidized Inconel was used in calculating external and internal radiation until the emissivity of the unoxidized Inconel equalled that of the oxidized Inconel, and then the emissivity of oxidized Inconel was used. Emissivity values above 2,000° F were obtained by linear extrapolation of the experimental data. The aerodynamic heat-transfer coefficients were nondimensionalized to obtain the Stanton number. Throughout this procedure air was treated as a perfect gas; the ratio of specific heats was used as 1.4; the specific heat at constant pressure was used as 0.24 Btu/(lb)(°F); the Prandtl number was held constant at 0.75; and the viscosity was obtained from the relation $\frac{\mu_1}{\mu_2} = \left(\frac{T_1}{T_2}\right)^{0.76}$ (ref. 8). Local-flow conditions along the conical surface were calculated by using the tables of reference 8 and by applying the modified Newtonian theory to determine surface pressure. The modified Newtonian theory, which agreed well with experiment for a hemisphere at a Mach number of 6.8 in reference 9, was expressed as $C_p = C_{p,t} \sin^2\theta$. Time histories of the calculated ratios of local-flow conditions to free-stream-flow conditions are presented in figure 15.

Calculated stagnation temperatures obtained from the relation

$$T_t = T_\infty\left(1 + \frac{\gamma - 1}{2} M_\infty^2\right)$$

and adiabatic-wall temperatures obtained from the relation

$$T_{aw} = N_{Pr}^{1/2}\left(T_t - T_l\right) + T_l$$

are presented in figure 16. The stagnation temperature and the adiabatic-wall temperature reached maximum values of 20,081° F and 18,612° F, respectively, at the end of the flight test. The recovery factor was held constant at $N_{Pr}^{1/2}$ throughout these calculations.

Stanton numbers at each temperature measuring station are presented as time histories in figure 17 and begin at the time that the heat flux exceeded 1 Btu/(sec)(sq ft). The heat flux remained very low until about 88.4 seconds, as indicated by the slope of the temperature time histories in figures 10 and 11. Values of Stanton number calculated during the time of very low heat flux are subject to large possible errors; therefore, the only function of those values presented before 88.4 seconds is to indicate

the general magnitude of the Stanton number. The remaining discussion of experimental data pertains to times later than 88.4 seconds ($M \approx 4.7$).

Three sets of theoretical Stanton numbers are also included in figure 17 for comparison with experimental values. Values of the local skin-friction coefficient from Van Driest's turbulent flat-plate theory using the Von Kármán mixing-length expression were obtained by use of the method and charts of reference 10 and were converted to values of Stanton number by the Reynolds analogy relation

$$N_{St} = 0.6C_f$$

as suggested in reference 11.

The theory of Van Driest (ref. 12) was then applied to calculate Stanton numbers for laminar flow. The flat-plate Stanton numbers were modified by multiplying them by $\sqrt{3}$ to obtain Stanton numbers along the conical surface. Because of the absence of enough information on the thermal properties of air at the high local temperatures encountered during the test, up to 9,200° F, the local Mach number, Reynolds number (based on distance from the stagnation point), and temperature applied to obtain theoretical Stanton numbers from the theories of Van Driest were calculated by assuming that the air behaved as a perfect gas (as previously noted).

Additional theoretical values of Stanton number for laminar flow, obtained by reducing the theoretical heat-flux values presented in figure 13 (obtained from refs. 5 and 6) in the manner used to reduce the experimental values, are also presented in figure 17. These values differed from the values obtained from the Van Driest laminar-flow theory, being only about three-fifths as large at the forward temperature measuring station (station 1). It may be noted, however, that the agreement between the laminar-flow theories improved as the distance from the stagnation point increased.

A comparison between experimental and theoretical Stanton numbers indicates that, in general, the flow along the conical nose was laminar until near the end of the test, with the exception of a burst of turbulence occurring at stations 3, 4, 5, and 6. The maximum values during the burst of turbulence were attained as the propellant in the fourth-stage rocket motor was ignited at 88.6 seconds at which the free-stream Mach number was 4.7 and the free-stream Reynolds number per foot was $0.603 \times 10^6$.

At the forward temperature measuring station (station 1), laminar flow existed during the entire time of the test as indicated by the

agreement between experimental and theoretical laminar-flow values from references 5 and 6. Free-stream Mach number and Reynolds number per foot increased to maximum values of 15.5 and $1.884 \times 10^6$, respectively, at the end of the test.

The flow at the second temperature measuring station was laminar until near the end of the test when the experimental Stanton numbers increased rapidly to the theoretical turbulent level.

Flow behavior at stations 3 to 6 was similar. After the burst of turbulence, previously mentioned, the flow at each station returned for a short time to about the laminar-flow level predicted for the cone by flat-plate theory. At about 90.5 seconds, the time when the propellant in the fifth-stage rocket motor was ignited, the flow was transitional with free-stream Mach number and Reynolds number per foot of 11.0 and $1.400 \times 10^6$, respectively. Soon after, the flow became turbulent for the rest of the flight test.

Extremely high values of Stanton number are indicated for most of the temperature measuring stations at the very end of the test. The experimental temperature measurements from which these high Stanton numbers were obtained appeared correct; however, other factors could possibly contribute to these high values. Inside and outside skin temperatures indicate that the nose was very near its melting temperature on the inside and probably was melting on the outside. Under these conditions it is conceivable that by the end of the flight test the nose skin had distorted under the influence of aerodynamic loads, thus changing the local conditions, and that either some of the nose material had melted or otherwise been lost or both. Loss of material would be reflected through the heat-balance relation as an apparent increase in the local heat transferred to the nose.

The local Stanton numbers could also be affected by a change in flow symmetry because of an angle of attack. Accelerometers mounted near the center of gravity of the model measured accelerations resulting from external forces acting on the model 90° apart in a position normal to the model center line. With these measurements, the resultant angle of attack has been estimated to have been a maximum of 15° at fifth-stage ignition. The angle of attack then decreased until near the end of the test when it reached an estimated 8.5° at $t = 92.1$ seconds. At the end of the test the angle of attack was about 10°. These angles of attack, which existed to some extent throughout the fifth-stage burning, were unanticipated because of the symmetry of the model. Orientation of the thermocouples with the calculated relative wind vector indicated that the line of thermocouples was not directly on the windward side but oscillated mostly in a range between 30° and 45° from the windward side during fifth-stage burning.

Although not conclusive, preliminary unpublished test results indicate that transition can possibly be started on bodies in hypersonic flight at angles of attack at locations 30° to 40° away from the windward side. This could possibly explain why transition occurred at 90.5 seconds at most of the temperature measuring stations.

## CONCLUDING REMARKS

Temperature measurements have been made on the inside surface of a blunted conical nose with a total angle of 29° that was tested on a rocket-propelled model which was flown to a maximum free-stream Mach number of 15.5 at an altitude of 98,200 feet. The temperature measurements were made at six stations along the inside surface of the cone, which was fabricated from Inconel, and reached a maximum temperature of 2,470° F at the end of the test.

Maximum heat flux was about 1,000 Btu/(sec)(sq ft) at all temperature measuring stations except at the most forward and the next-to-last stations which had 700 and 1,650 Btu/(sec)(sq ft), respectively. The experimental heat flux at the first temperature measuring station agreed well with theoretical values obtained for laminar, equilibrium, dissociated flow, but the experimental values became increasingly greater than the theoretical values at the more rearward temperature measuring stations.

When compared with Stanton numbers obtained from turbulent- and laminar-flow theories by applying perfect-gas relations, the experimental Stanton numbers, likewise obtained by applying perfect-gas relations, indicated that the flow was laminar at the two forward temperature measuring stations except at the second station near the end of the test. Also, the flow at the other stations followed a pattern that indicated the presence of laminar flow that was interrupted by a burst of turbulence, of transitional flow beginning at a free-stream Mach number and Reynolds number per foot of 11.0 and $1.4 \times 10^6$, respectively, and of turbulent flow near the end of the test.

Extremely high Stanton numbers obtained at the end of the test when the nose skin was close to the melting temperature are believed to have been caused by either nose distortion or surface disfiguration or both.

Langley Aeronautical Laboratory,
National Advisory Committee for Aeronautics,
Langley Field, Va., June 17, 1957.

## REFERENCES

1. Piland, Robert O.: Performance Measurements From a Rocket-Powered Exploratory Research Missile Flown to a Mach Number of 10.4. NACA RM L54L29a, 1955.

2. Bland, William M., Jr., and Collie, Katherine A.: Free-Flight Aerodynamic-Heating Data to Mach Number 10.4 for a Modified Von Kármán Nose Shape. NACA RM L56D25, 1956.

3. Bond, Aleck C., and Rumsey, Charles B.: Free-Flight Skin Temperature and Pressure Measurements on a Slightly Blunted 25° Cone-Cylinder-Flare Configuration to a Mach Number of 9.89. NACA RM L57B18, 1957.

4. Stoney, William E., Jr., and Swanson, Andrew G.: Heat Transfer Measured on a Flat-Face Cylinder in Free Flight at Mach Numbers Up to 13.9. NACA RM L57E13, 1957.

5. Fay, J. A., and Riddell, F. R.: Stagnation Point Heat Transfer in Dissociated Air. Res. Note 18, AVCO Res. Lab., June 1956.

6. Lees, Lester: Laminar Heat Transfer on Blunt-Nosed Bodies at Hypersonic Flight Speeds. Jet Propulsion, vol. 26, no. 4, Apr. 1956, pp. 259-269.

7. Ginnings, Defoe C., and Thomas, Eugenia: The Electrical Resistance and Total Radiant Emittance of Inconel in the Range 0° to 1000° C. NBS Rep. 4111 (NACA Contract S54-52), Nat. Bur. Standards, May 1955.

8. Ames Research Staff: Equations, Tables, and Charts for Compressible Flow. NACA Rep. 1135, 1953. (Supersedes NACA TN 1428.)

9. Crawford, Davis H., and McCauley, William D.: Investigation of the Laminar Aerodynamic Heat-Transfer Characteristics of a Hemisphere-Cylinder in the Langley 11-Inch Hypersonic Tunnel at a Mach Number of 6.8. NACA TN 3706, 1956.

10. Lee, Dorothy B., and Faget, Maxime A.: Charts Adapted From Van Driest's Turbulent Flat-Plate Theory for Determining Values of Turbulent Aerodynamic Friction and Heat-Transfer Coefficients. NACA TN 3811, 1956.

11. Rubesin, Morris W.: A Modified Reynolds Analogy for the Compressible Turbulent Boundary Layer on a Flat Plate. NACA TN 2917, 1953.

12. Van Driest, E. R.: Investigation of Laminar Boundary Layer in Compressible Fluids Using the Crocco Method. NACA TN 2597, 1952.

TABLE I

CHARACTERISTICS OF ROCKET MOTORS USED IN TEST

| Stage | Motor designation | Propellant weight, lb | Motor weight, lb | Stage weight, lb | Combination weight, lb | Average thrust, lb (a) | Burning time, sec (a) |
|---|---|---|---|---|---|---|---|
| 1 | M6 JATO "Honest John" | 2,050.0 | 3,874 | 4,099 | 7,156 | 83,300 | 4.4 |
| 2 | M5 JATO "Nike" | 740.0 | 1,180 | 1,312 | 3,057 | 45,000 | 3.1 |
| 3 | M5 JATO "Nike" | 740.0 | 1,180 | 1,283 | 1,745 | 45,000 | 3.1 |
| 4 | JATO, 1.52-KS-33,550,XM19 "Recruit" | 268.0 | 355 | 393 | 462 | 34,640 | 1.5 |
| 5 | JATO, 1.52-KS-4800-T55 | 33.6 | 46 | 69 | 69 | 4,360 | 1.6 |

[a]From manufacturer's specifications.

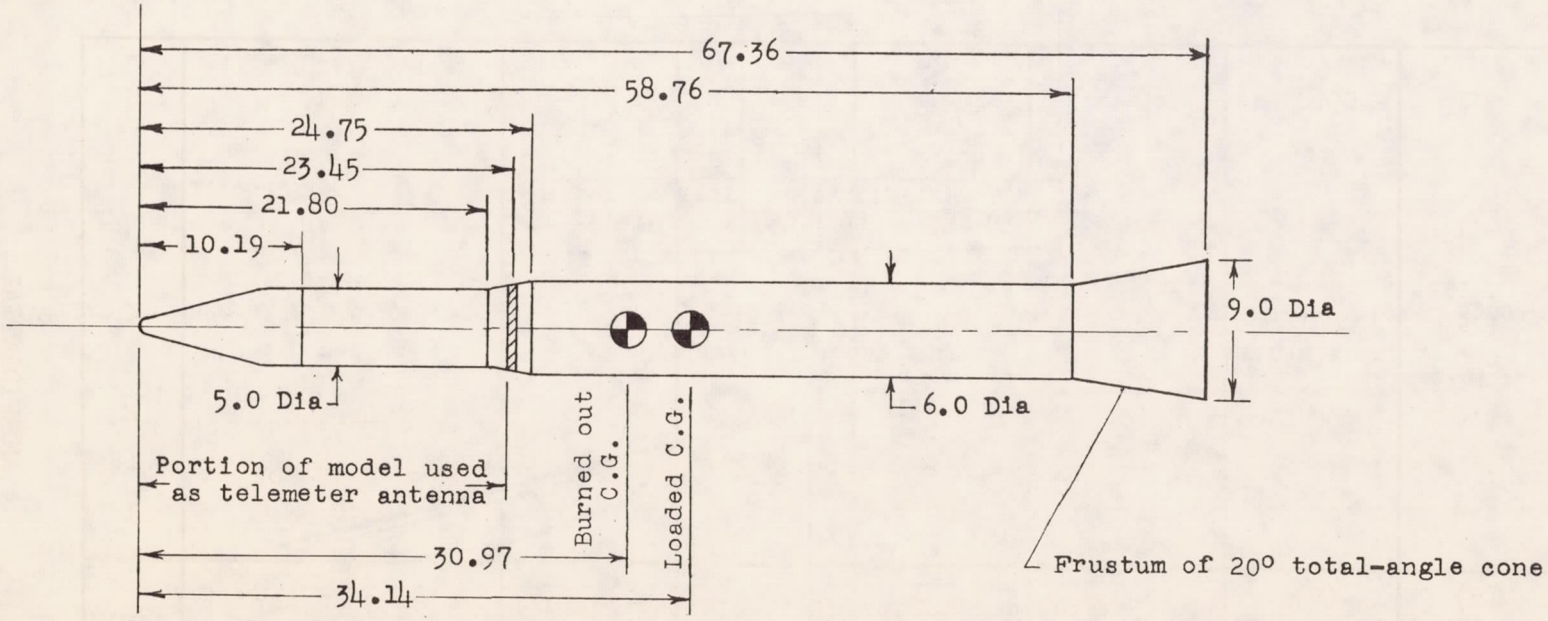


Figure 1.- Sketch of model (fifth stage). Dimensions are in inches.

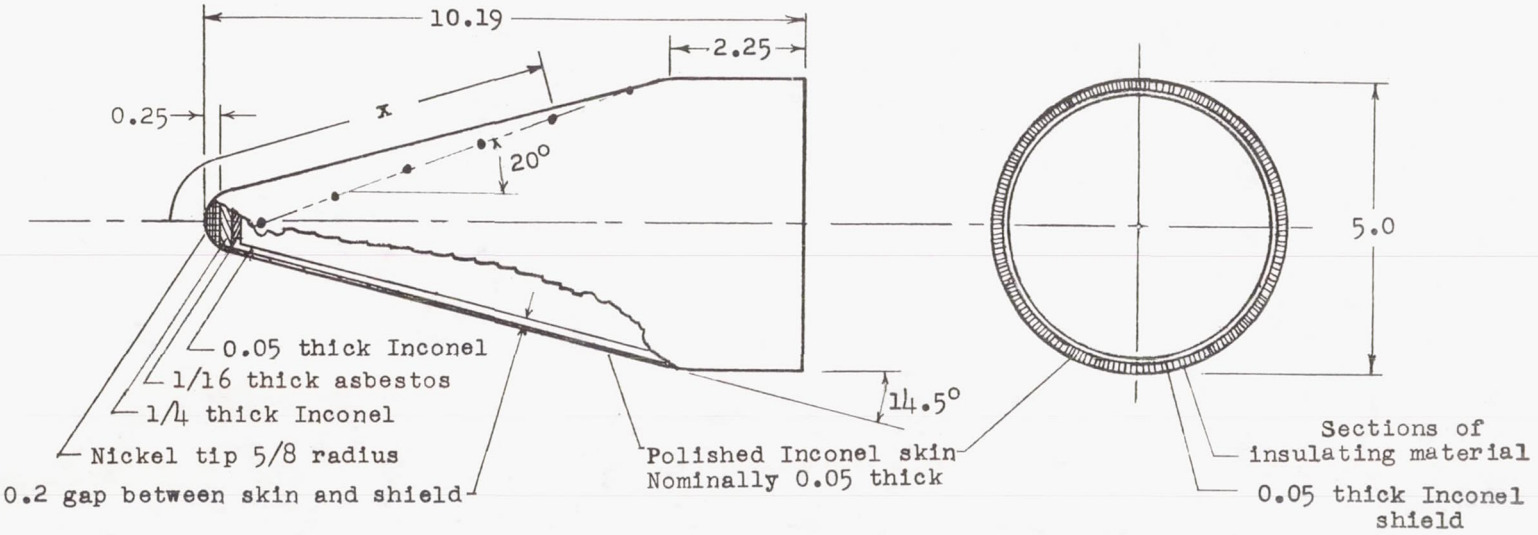


| Temperature measuring sta | x | Measured local skin thickness |
|---|---|---|
| 1 | 1.37 | 0.044 |
| 2 | 2.67 | .039 |
| 3 | 3.97 | .045 |
| 4 | 5.25 | .044 |
| 5 | 6.55 | .046 |
| 6 | 7.85 | .046 |

Figure 2.- Sketch of nose showing details and temperature measuring stations. Dimensions are in inches.

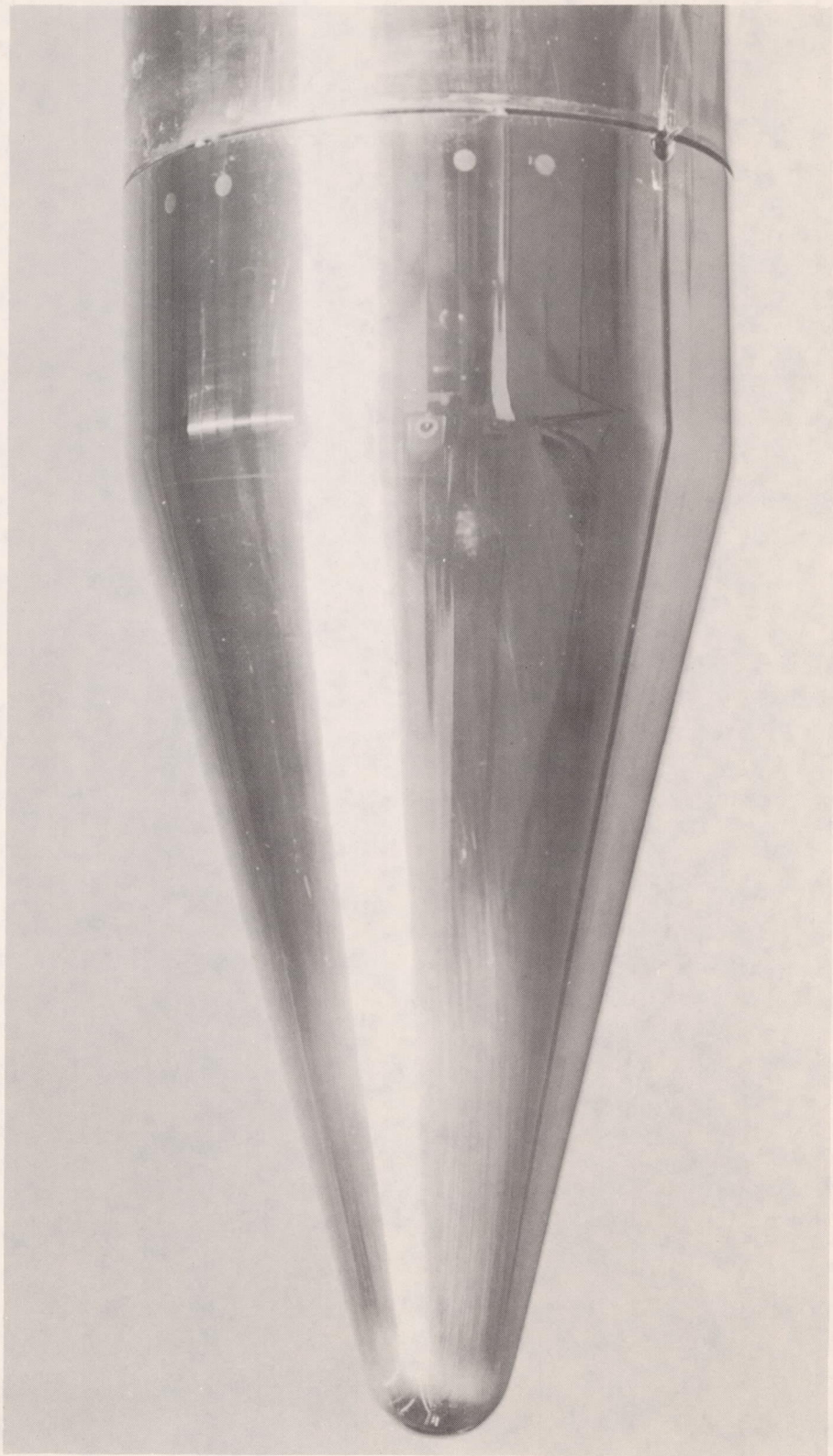

Figure 3.- Blunted nose cone. L-57-1013

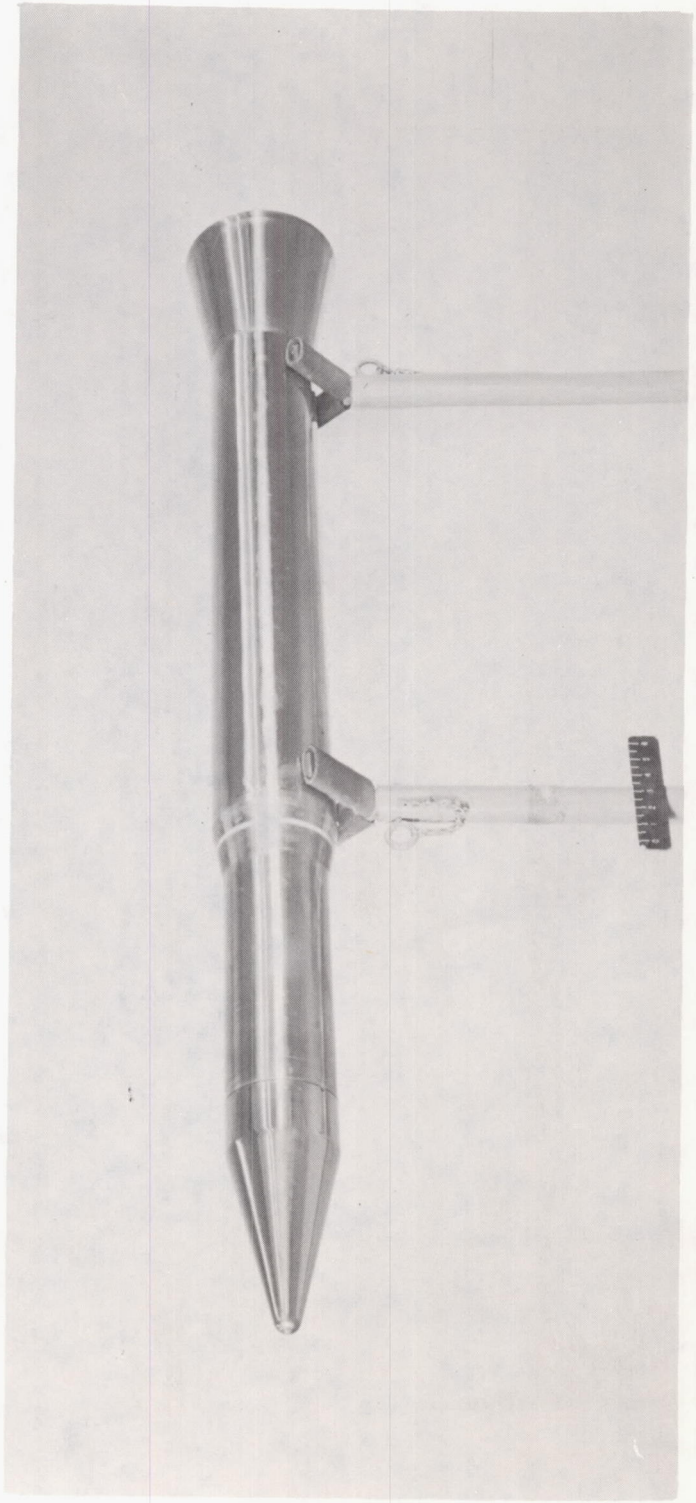

Figure 4.- Model (fifth stage). L-57-1011.1

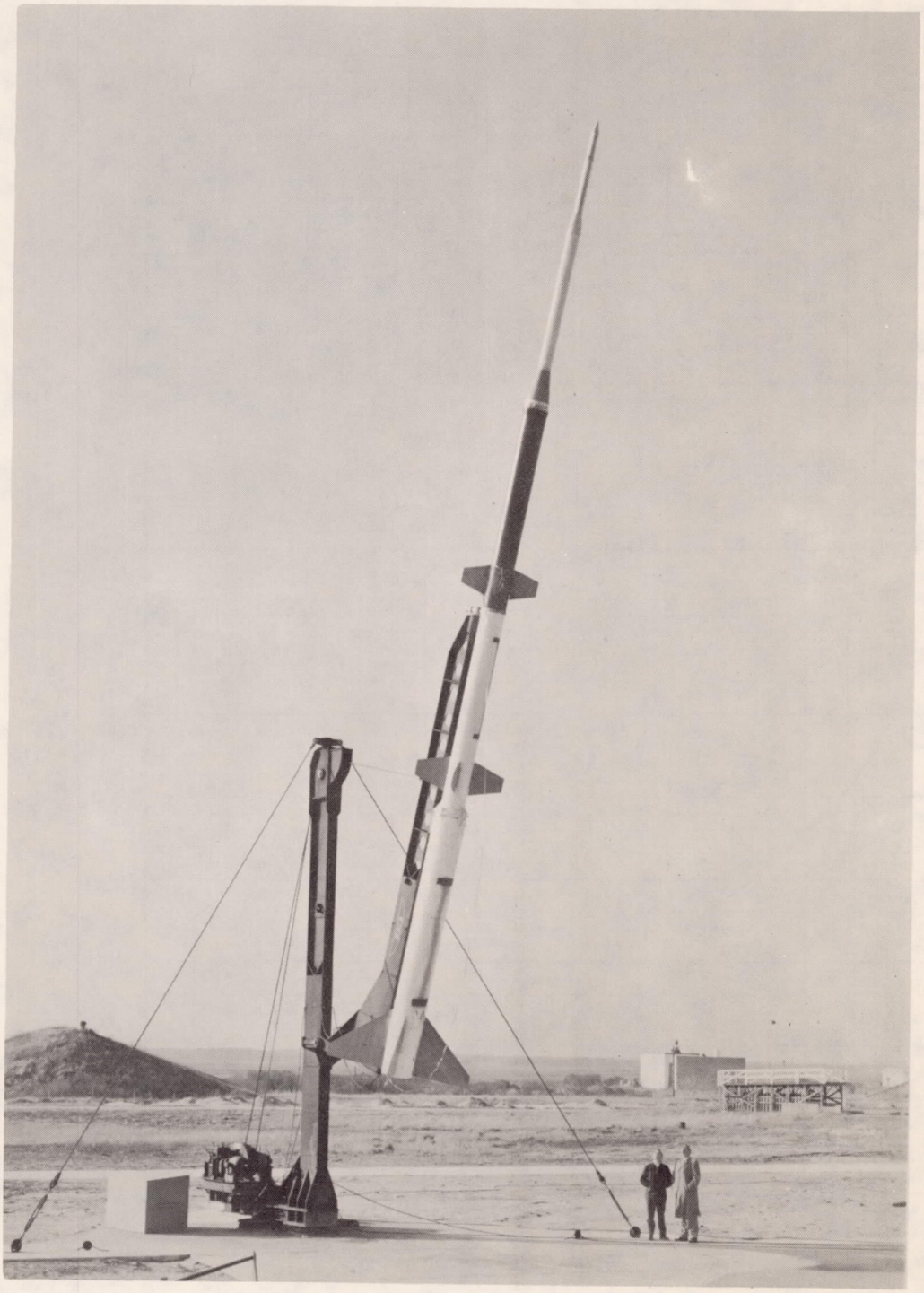

Figure 5.- Model and four booster stages on launcher. L-57-1241

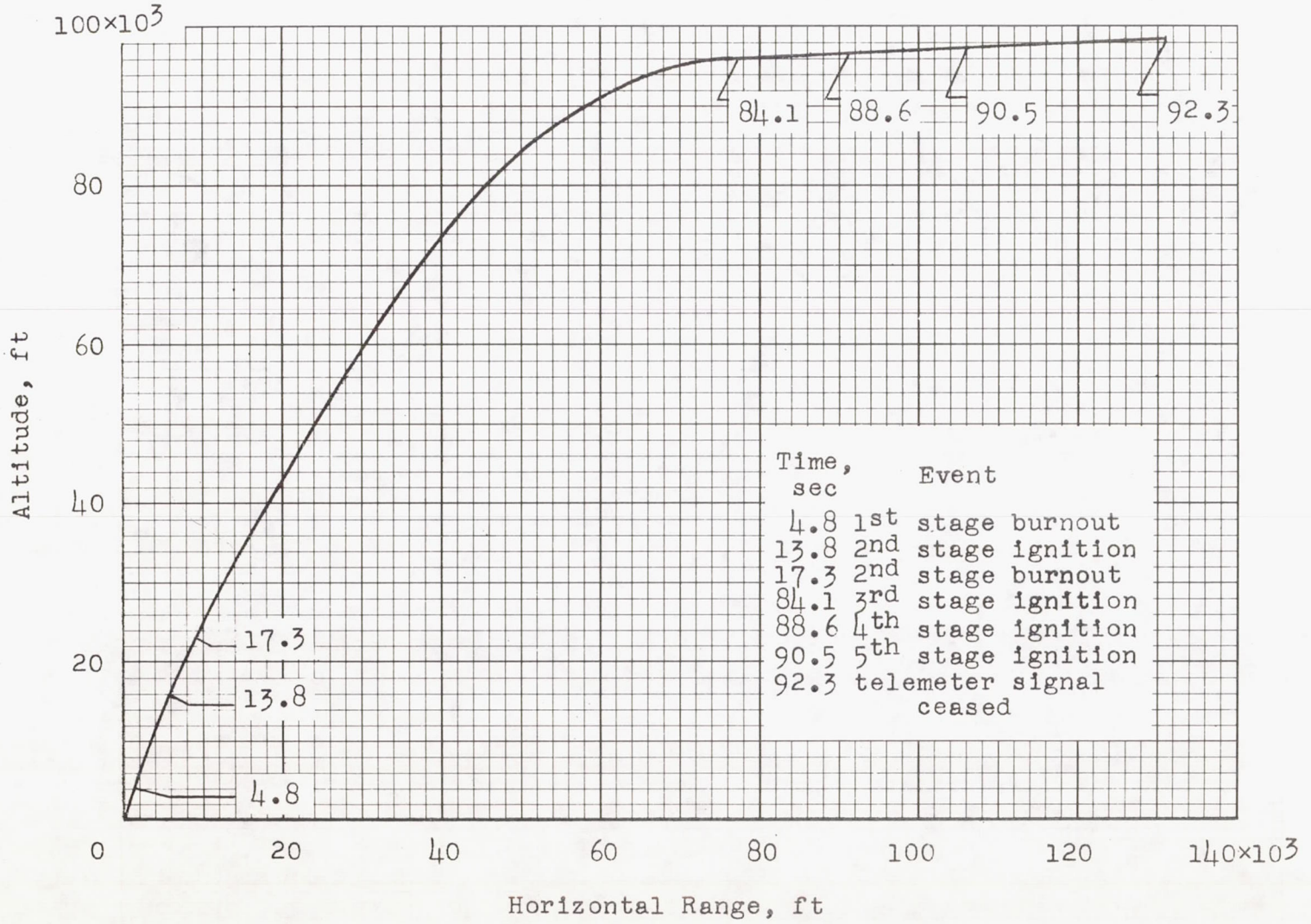


Figure 6.- Model trajectory to the time that the telemeter signal ceased.

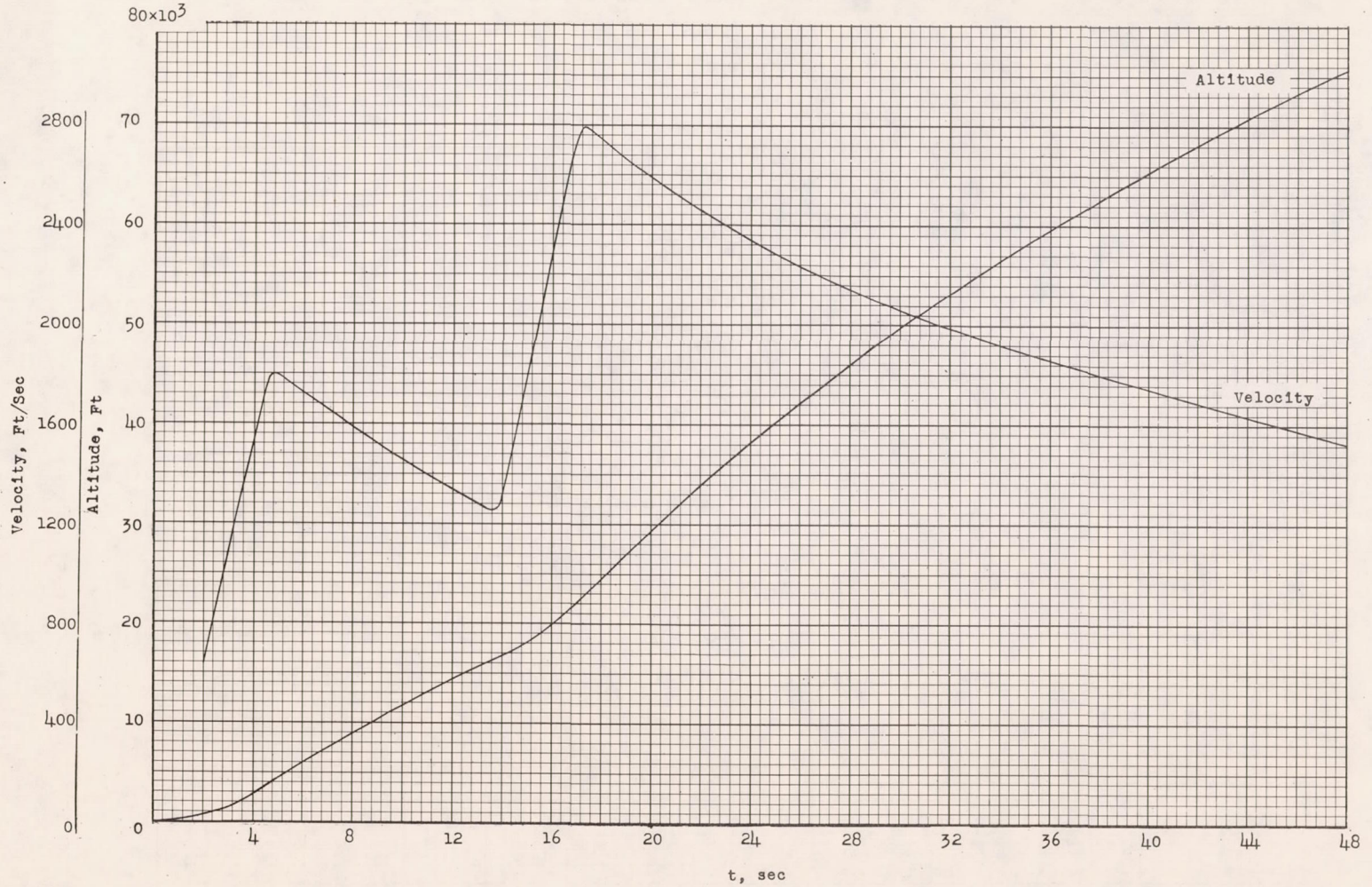


(a) 0 to 48 seconds.

Figure 7.- Time histories of altitude and free-stream velocity.

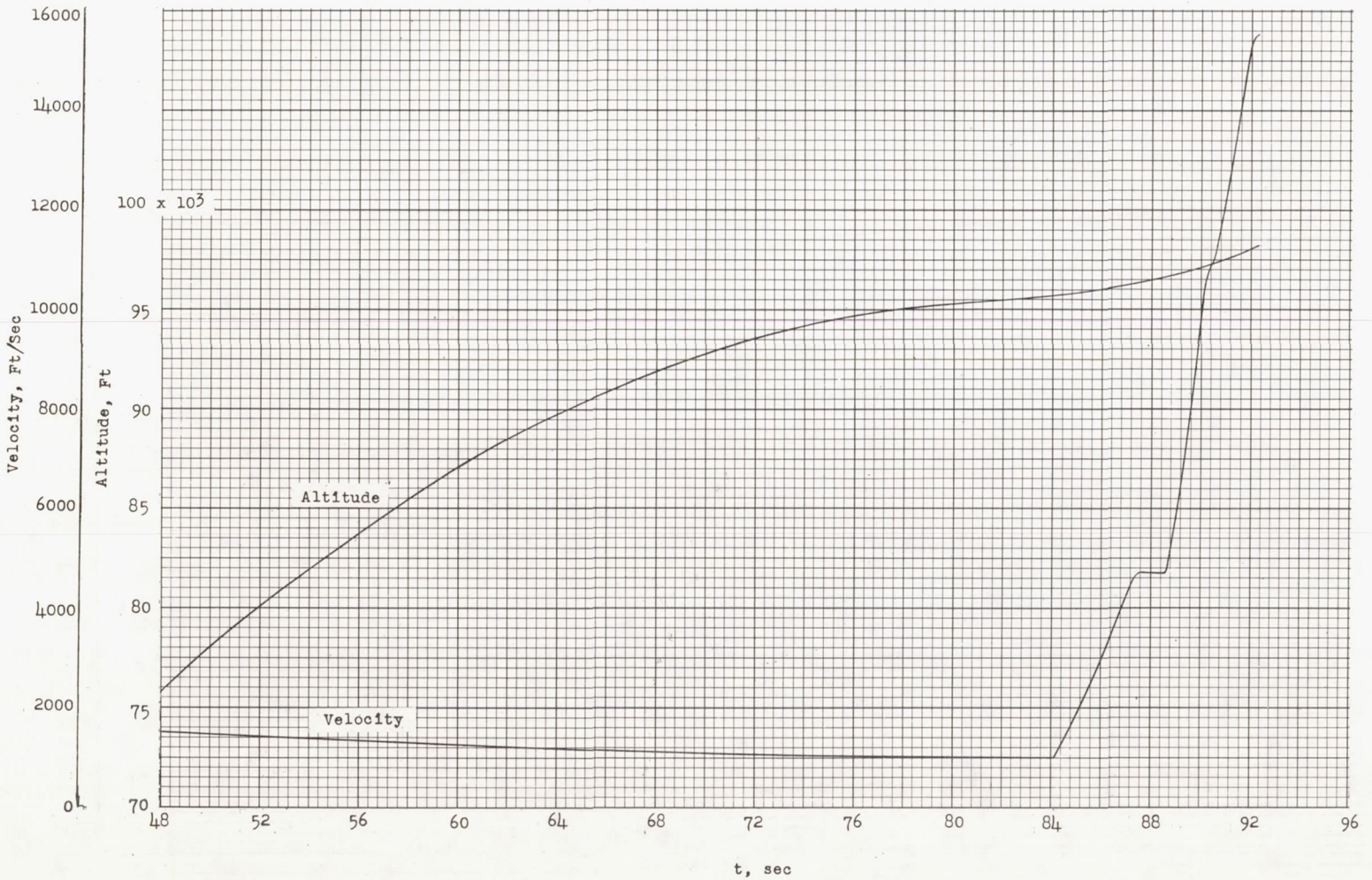


(b) 48 to 96 seconds.

Figure 7.- Concluded.

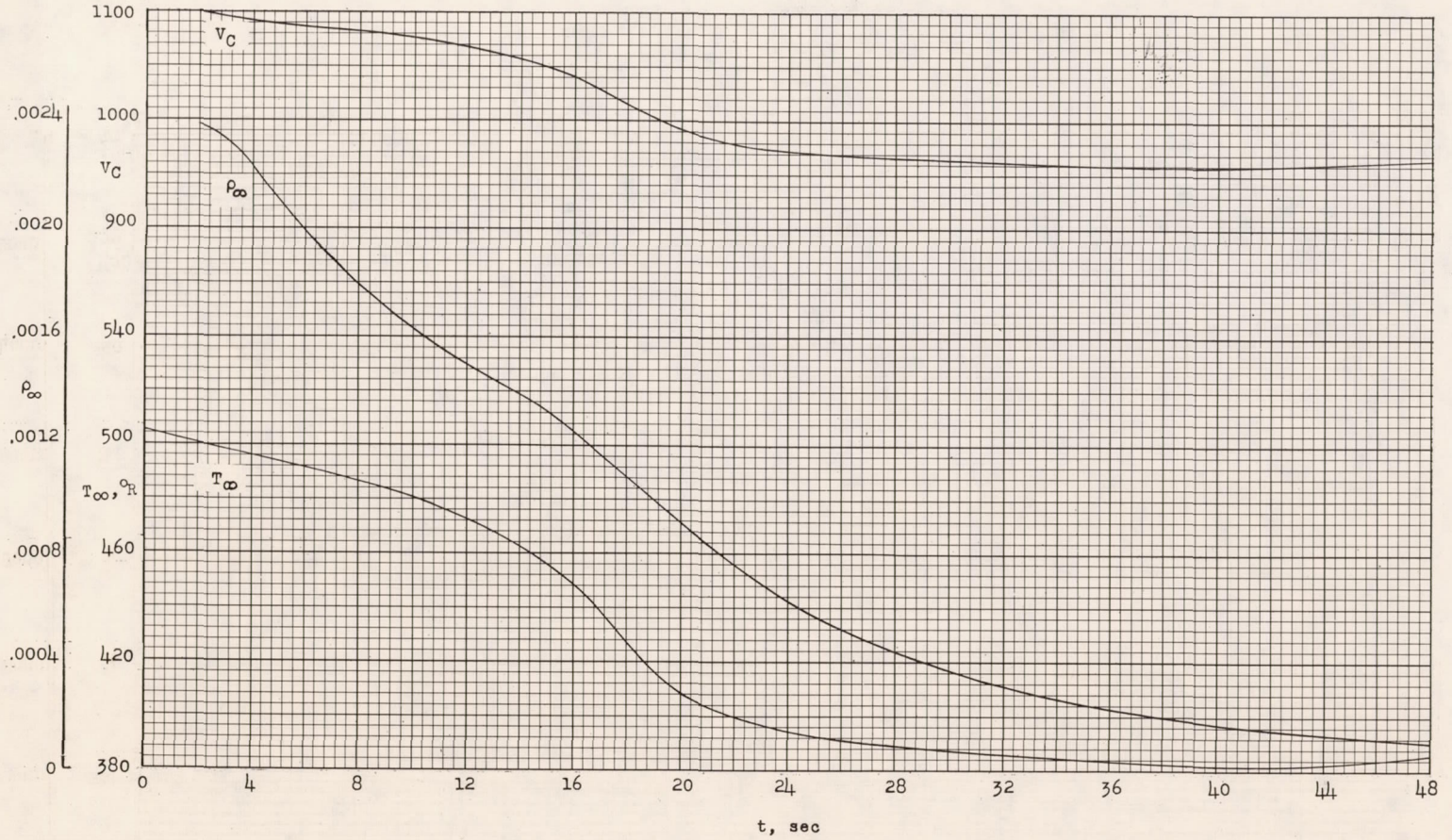


(a) 0 to 48 seconds.

Figure 8.- Time histories of atmospheric density, temperature, and velocity of sound.

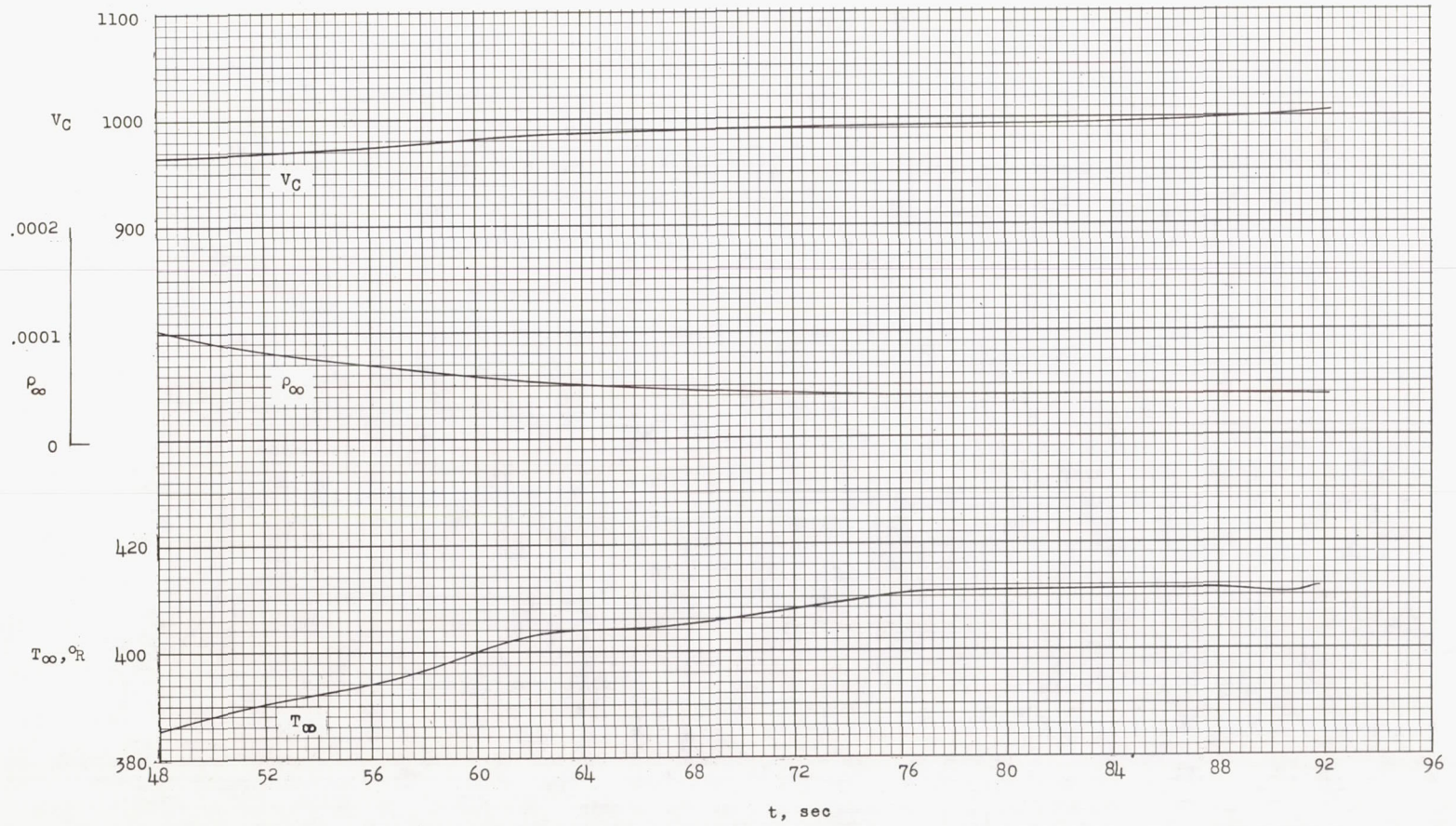


(b) 48 to 96 seconds.

Figure 8.- Concluded.

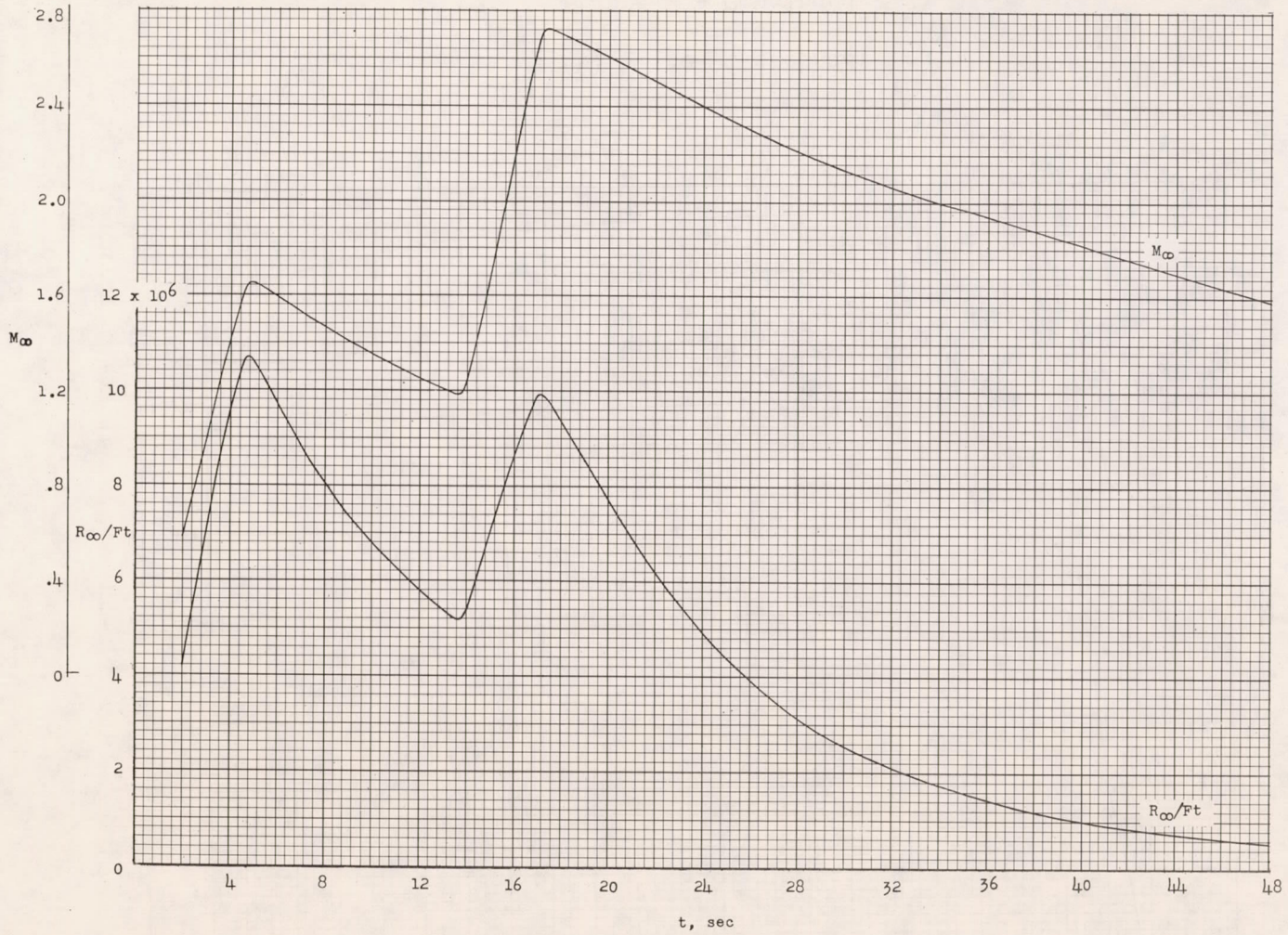


(a) 0 to 48 seconds.

Figure 9.- Time histories of free-stream Mach number and Reynolds number per foot.

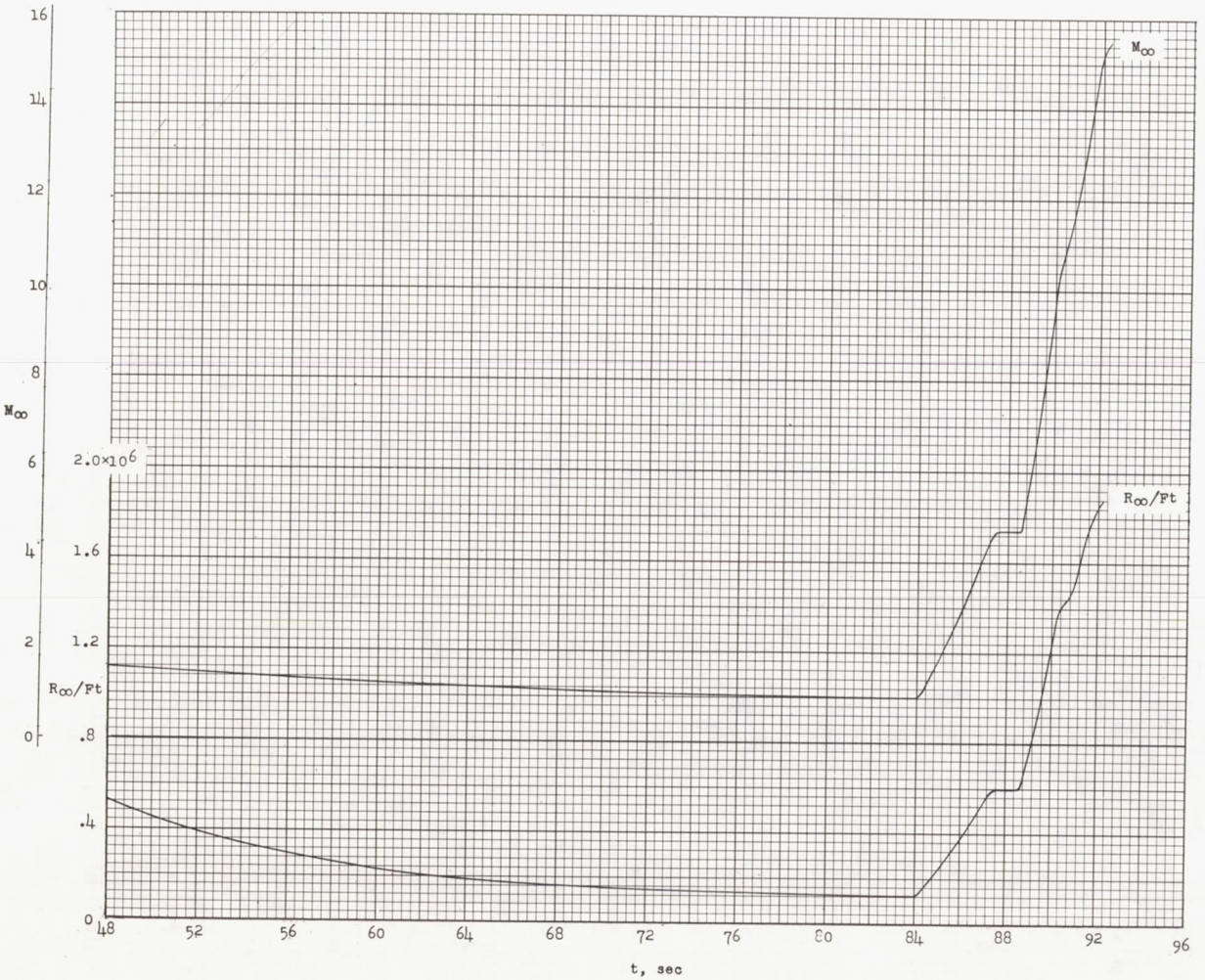


(b) 48 to 96 seconds.

Figure 9.- Concluded.

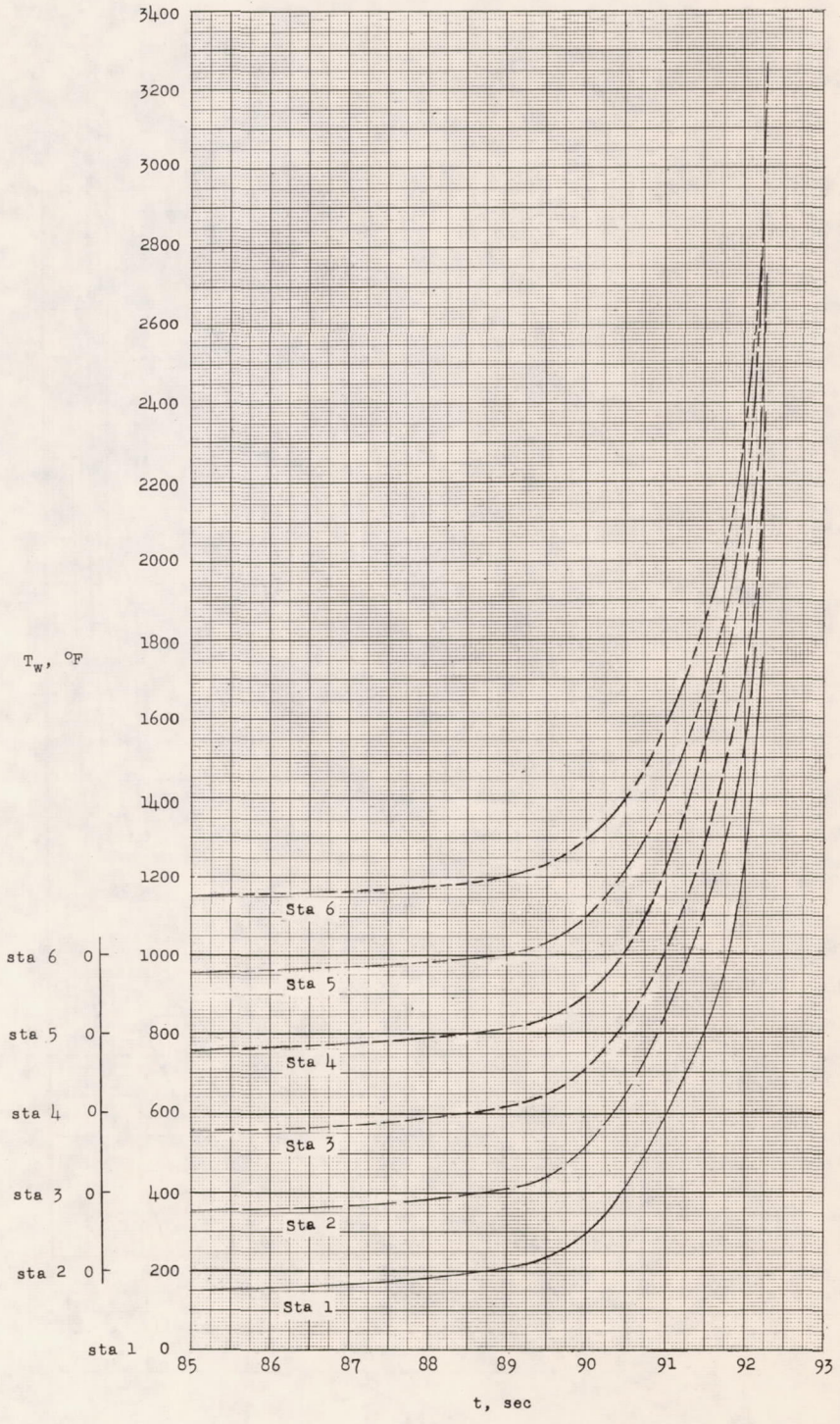


Figure 10.- Time histories of measured inside skin temperatures.

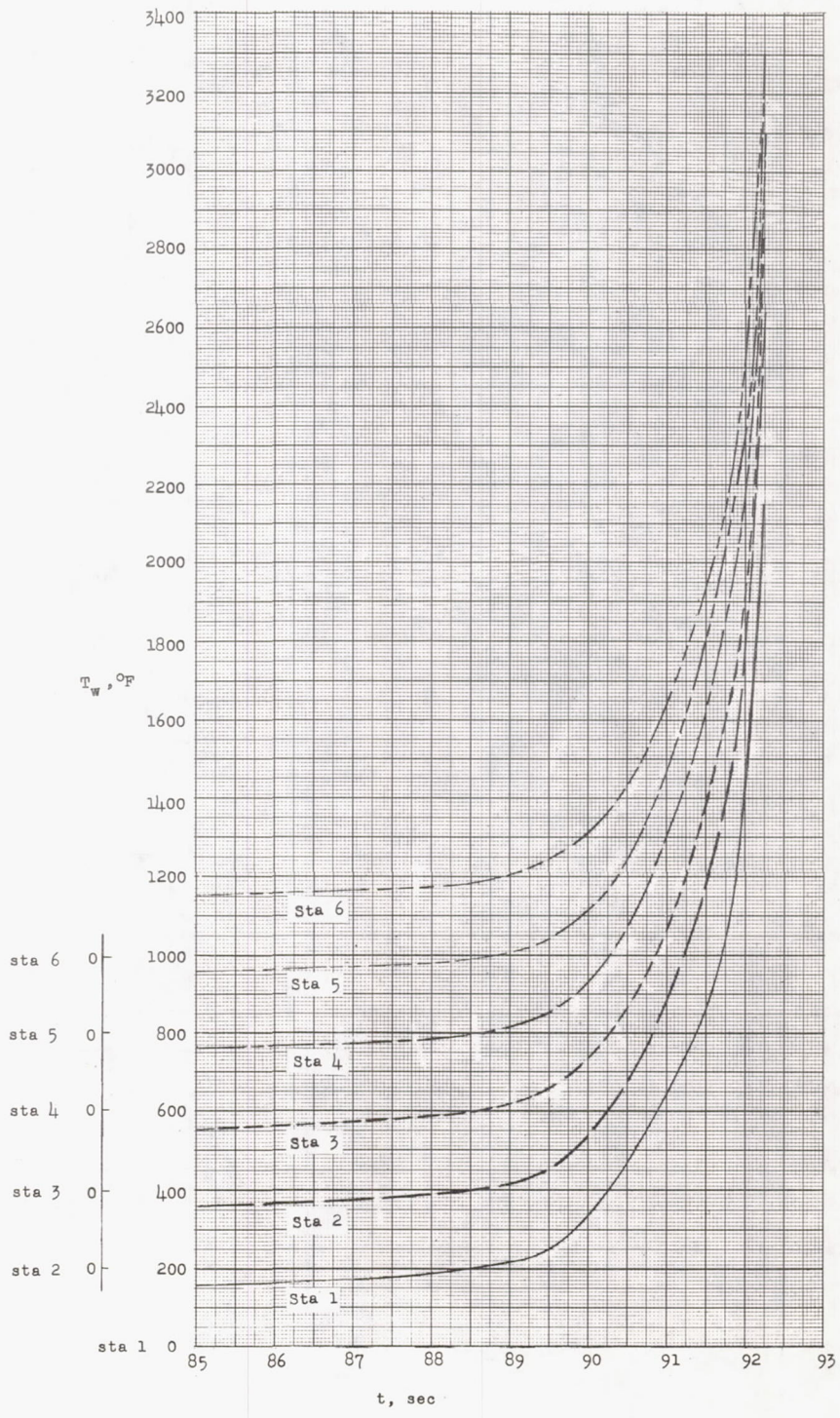


Figure 11.- Time histories of outside skin temperatures.

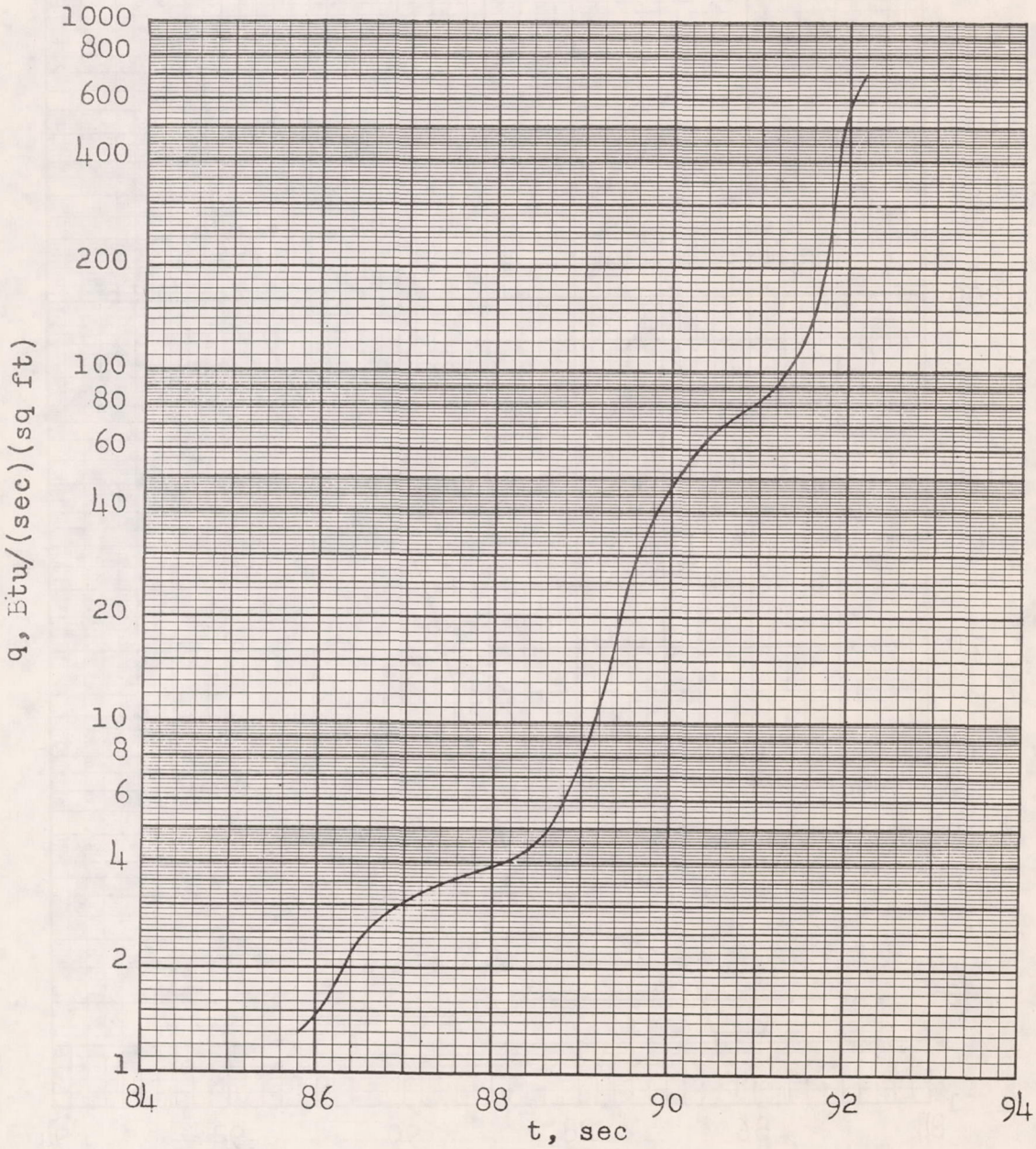


(a) Station 1 based on average temperature.

Figure 12.- Net heat flux plotted against time.

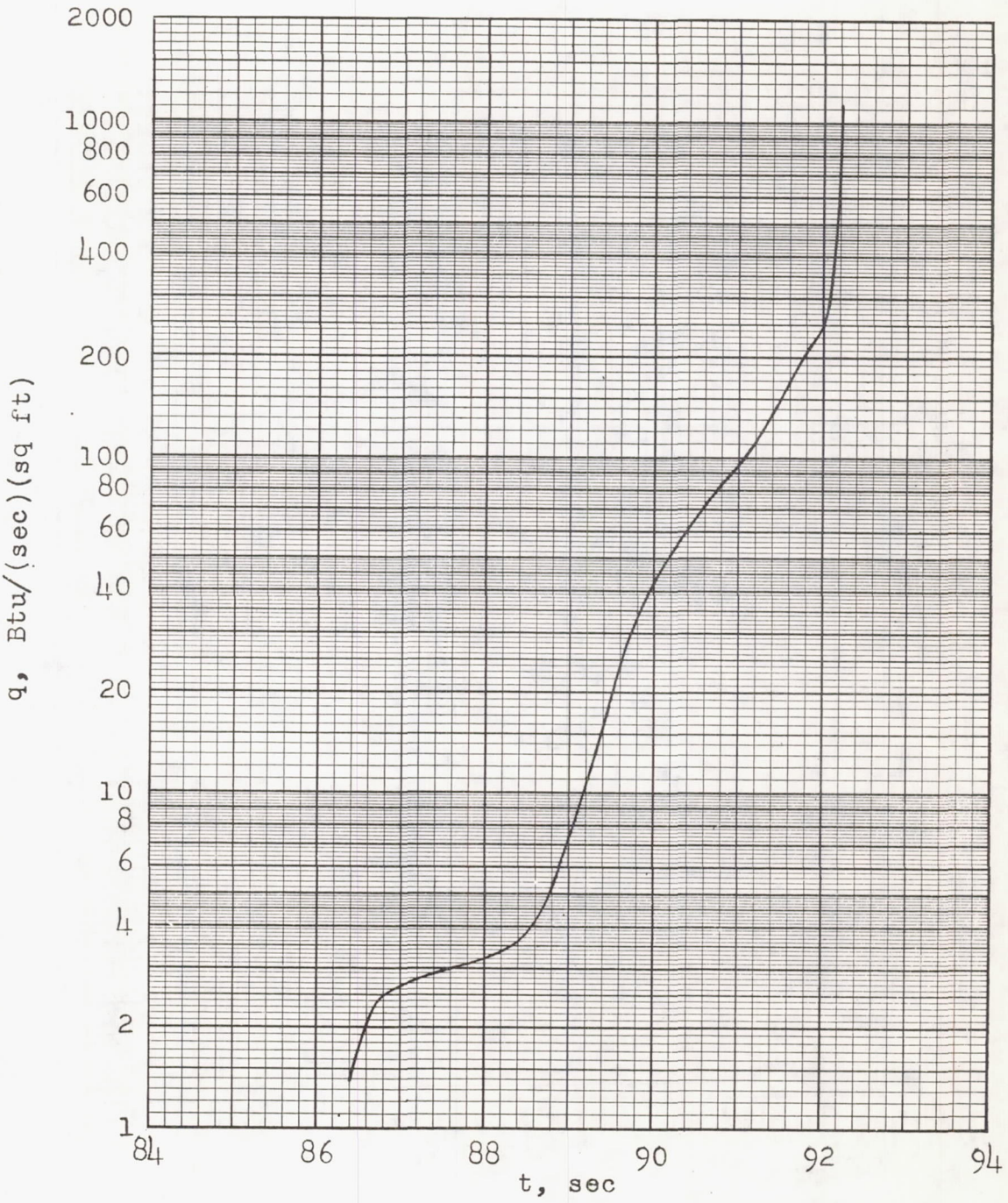


(b) Station 2 based on average temperature.

Figure 12.- Continued.

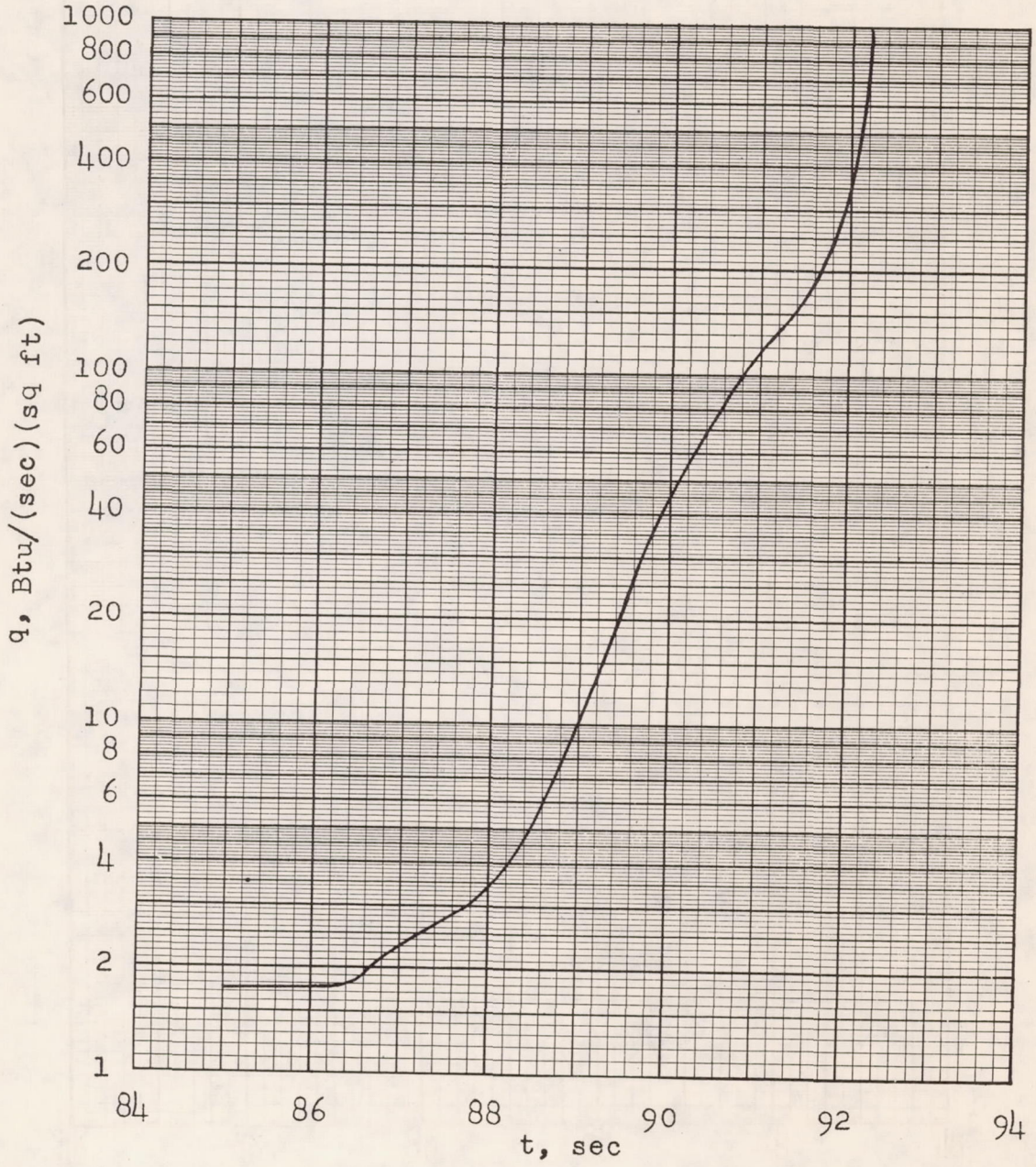


(c) Station 3 based on average temperature.

Figure 12.- Continued.

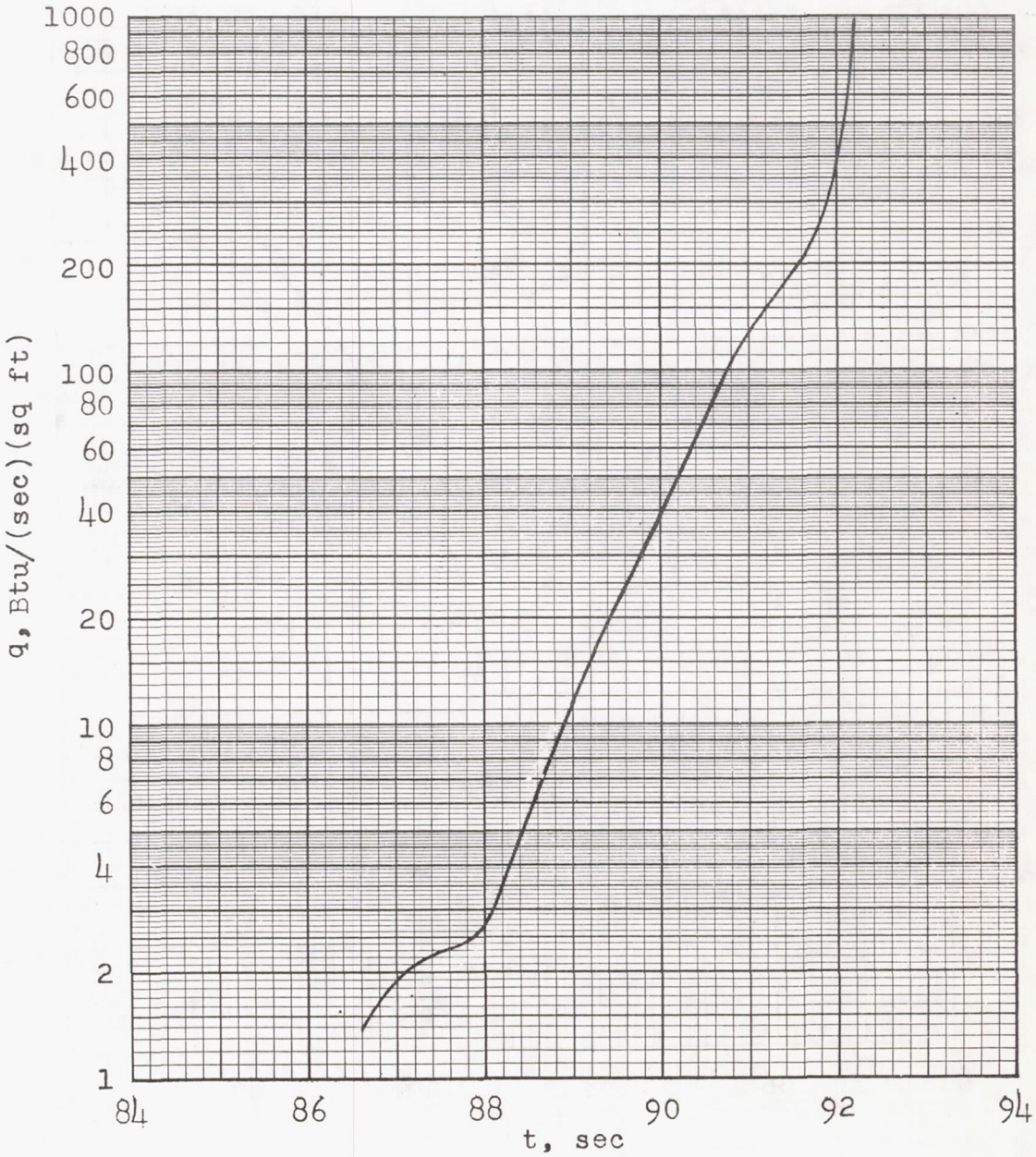


(d) Station 4 based on average temperature.

Figure 12.- Continued.

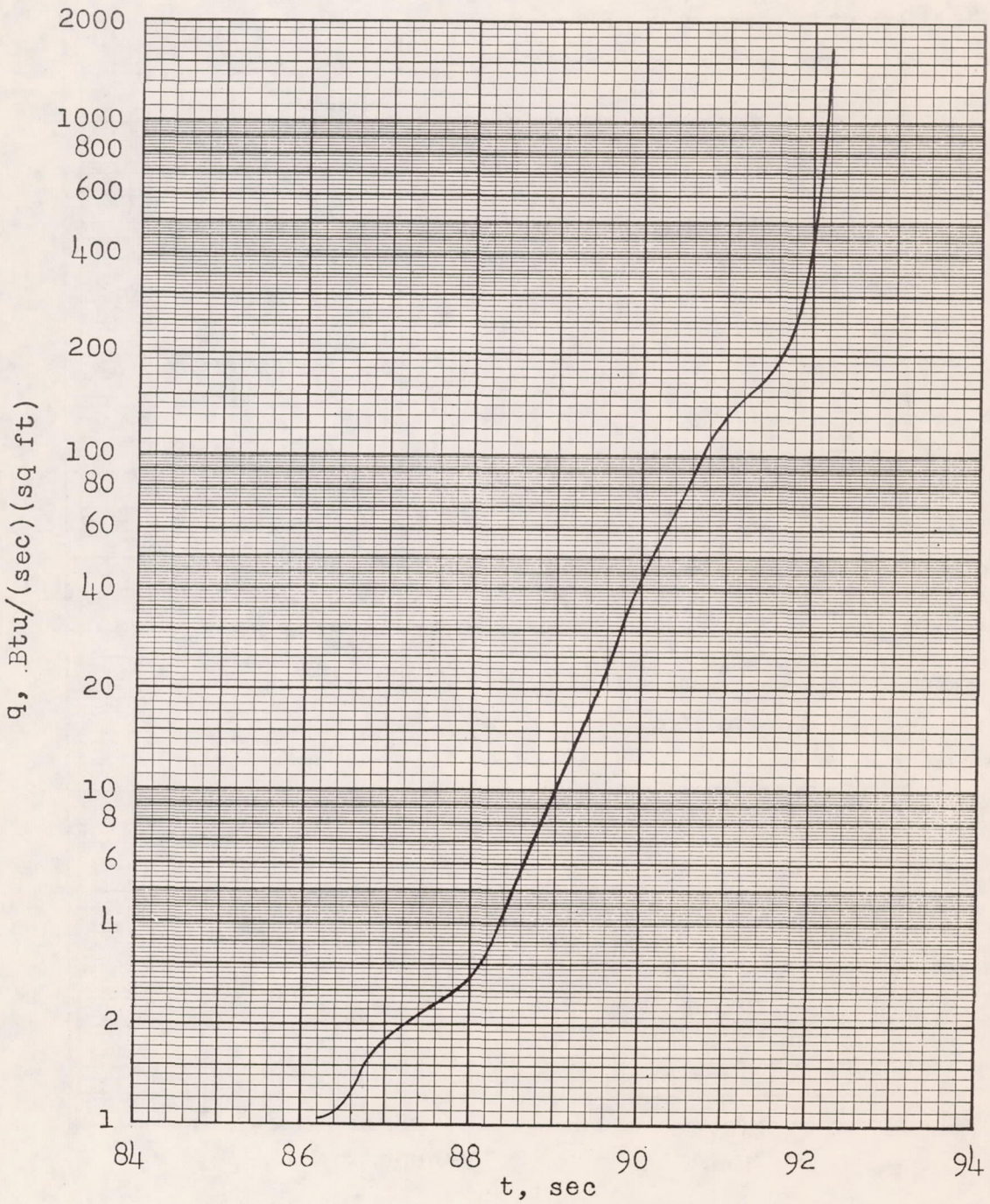


(e) Station 5 based on average temperature.

Figure 12.- Continued.

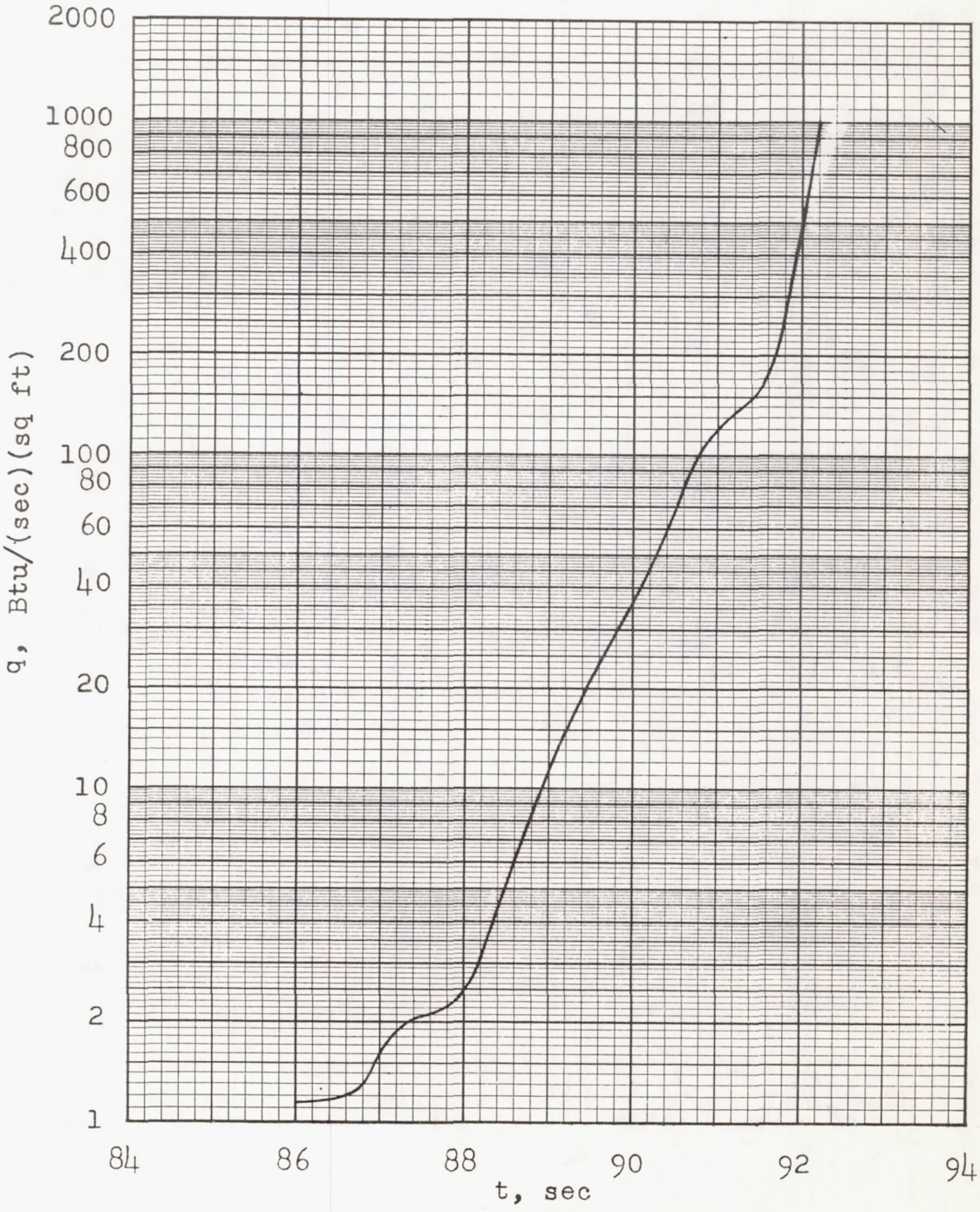


(f) Station 6 based on average temperature.

Figure 12.- Continued.

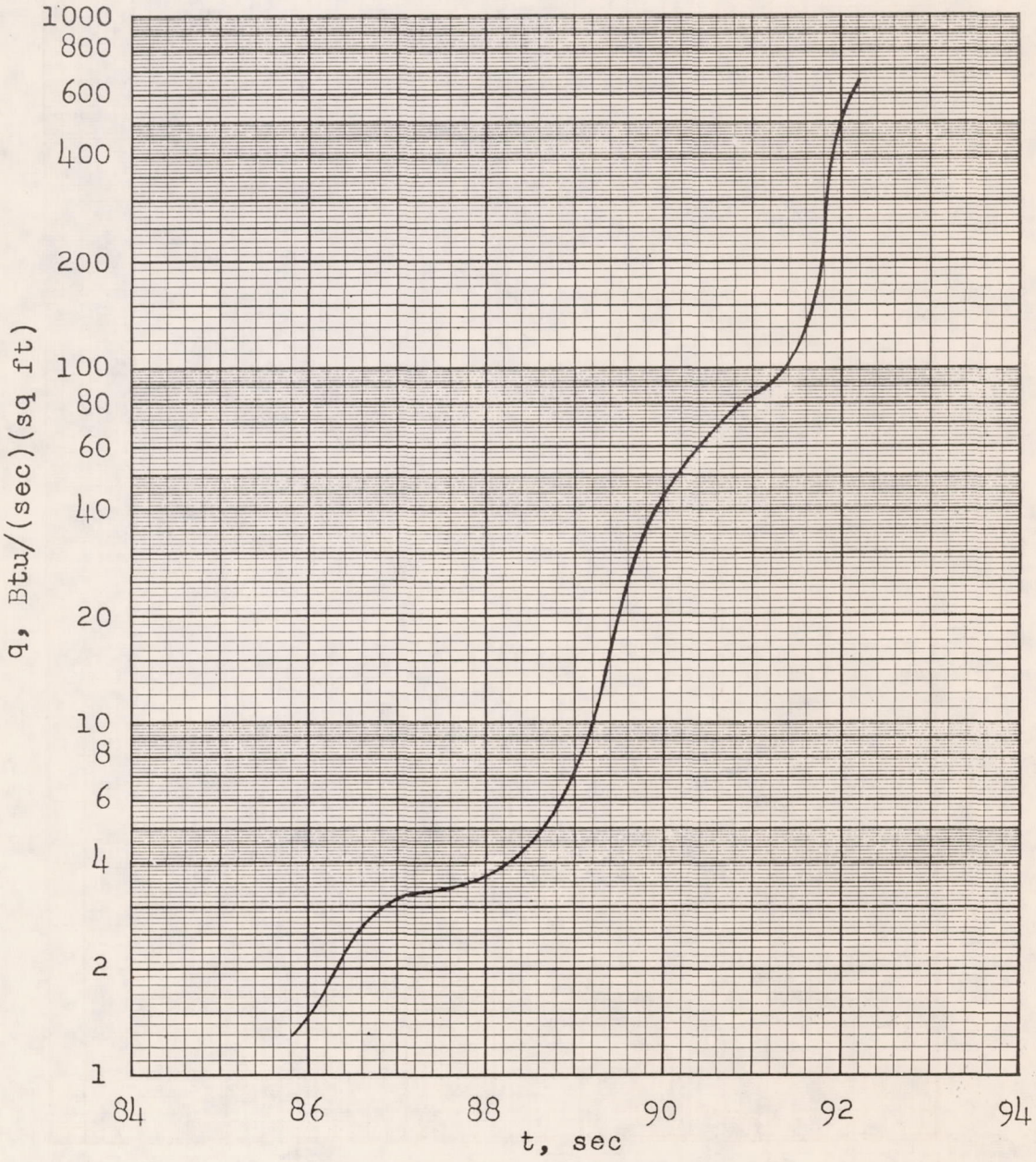


(g) Station 1 based on inside temperature.

Figure 12.- Concluded.

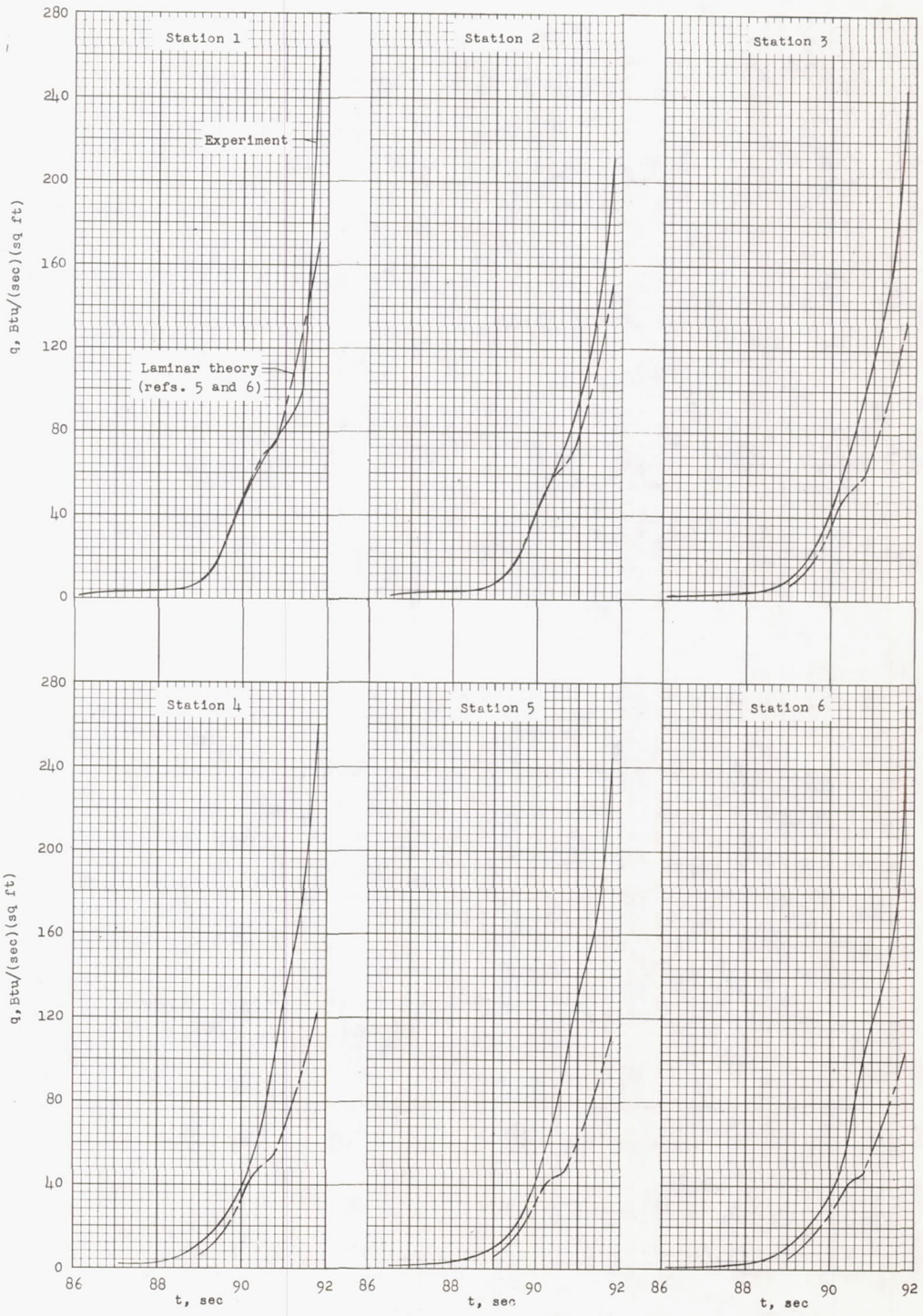


Figure 13.- Comparison of experimental and theoretical heat flux based on laminar dissociated flow (refs. 5 and 6).

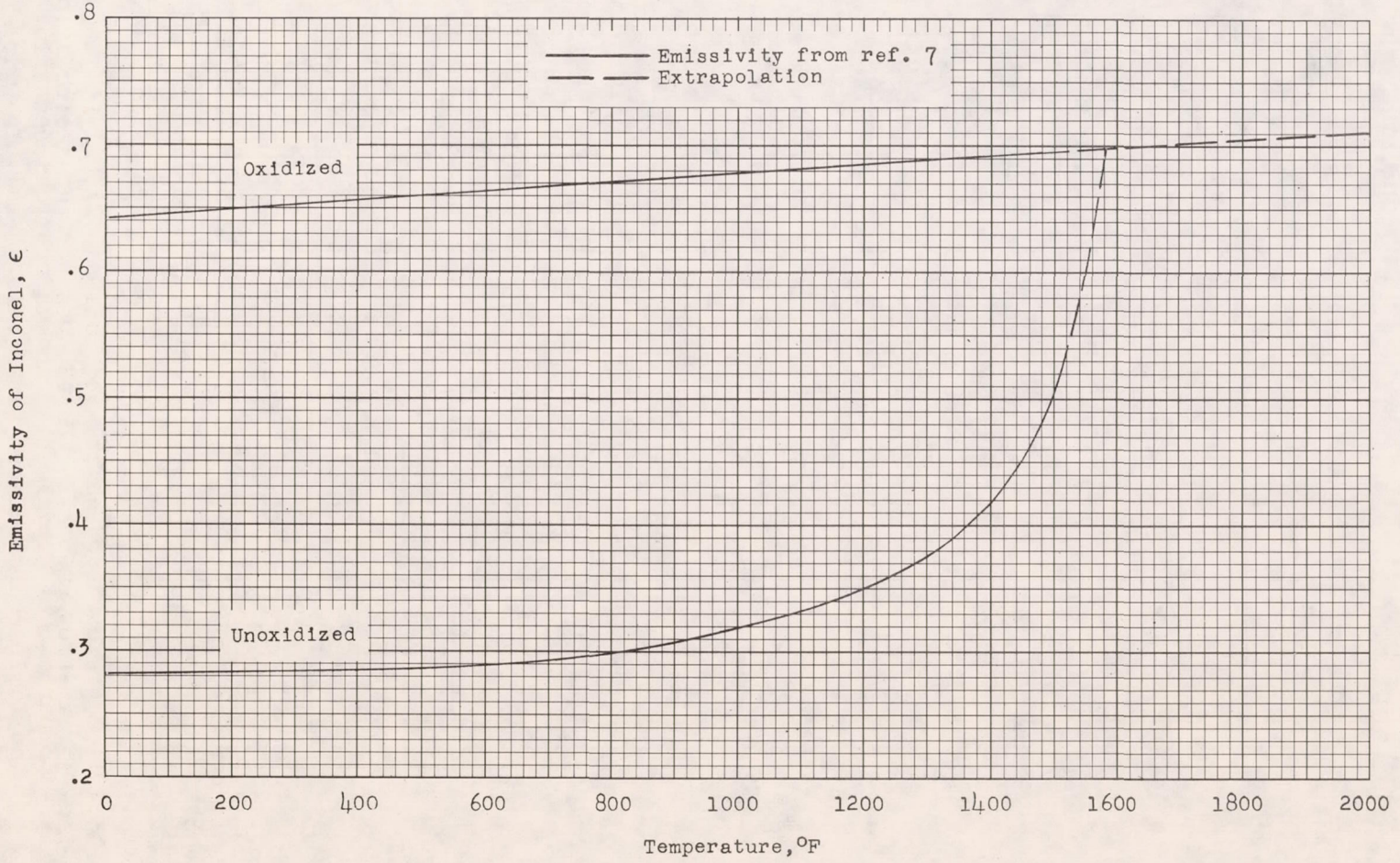


Figure 14.- Variation of emissivity of Inconel with temperature.

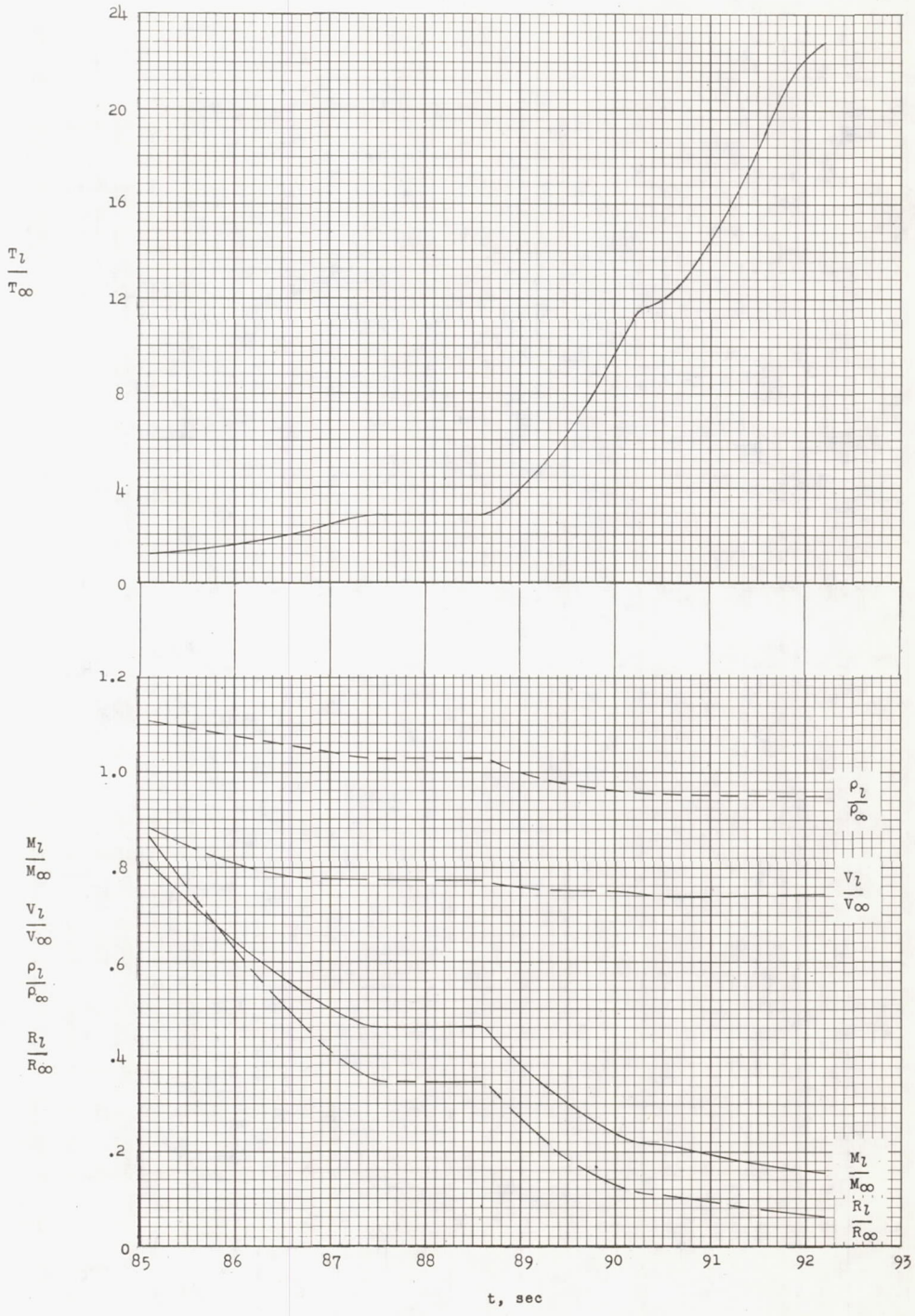


Figure 15.- Time histories of calculated ratios of local-flow properties to free-stream-flow properties based upon perfect-gas relations.

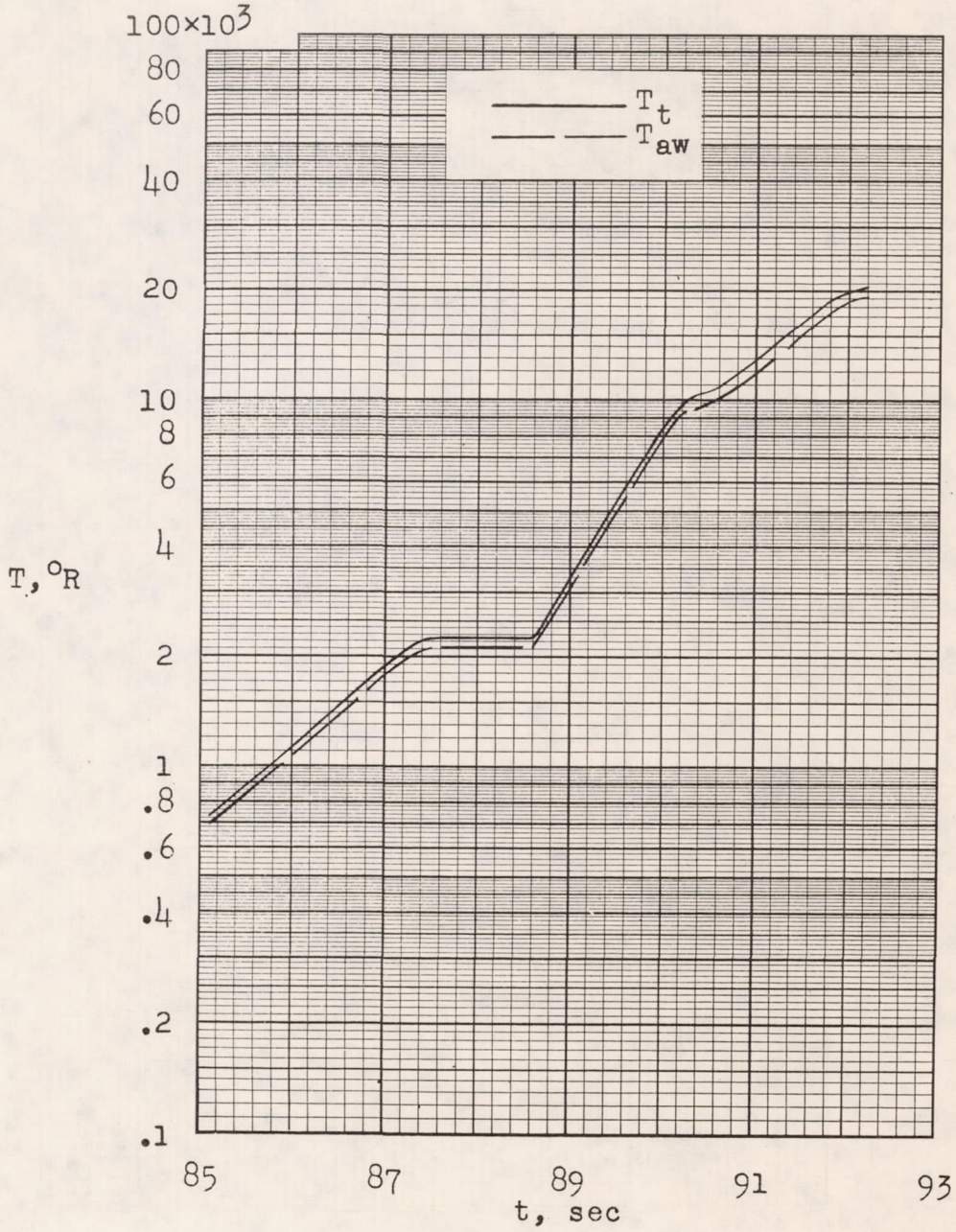


Figure 16.- Time histories of stagnation temperature and adiabatic-wall temperature based on perfect-gas relations. $N_{Pr} = 0.75$.

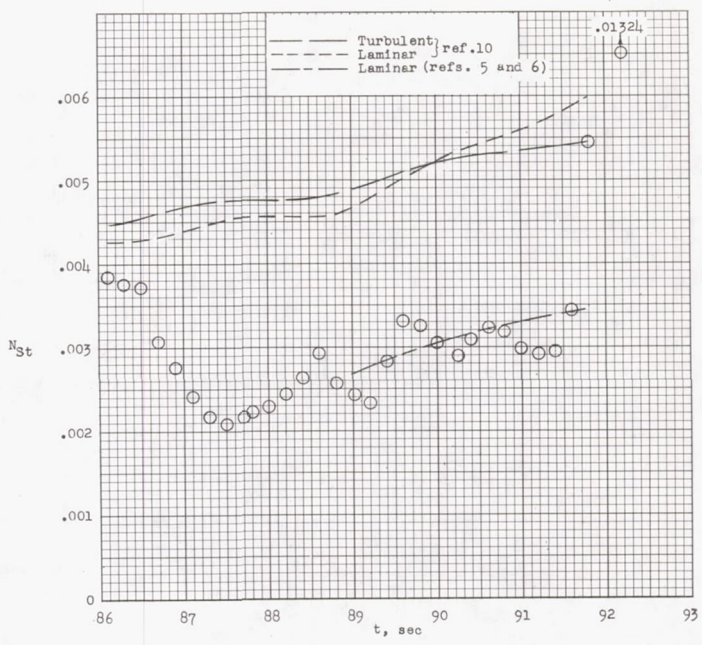


(a) Temperature measuring station 1.

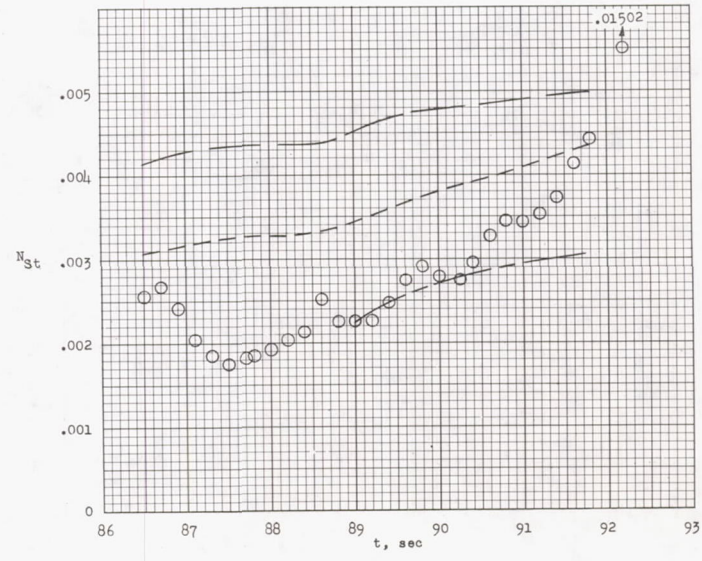


(b) Temperature measuring station 2.

Figure 17.- Time histories of experimental and theoretical Stanton numbers.

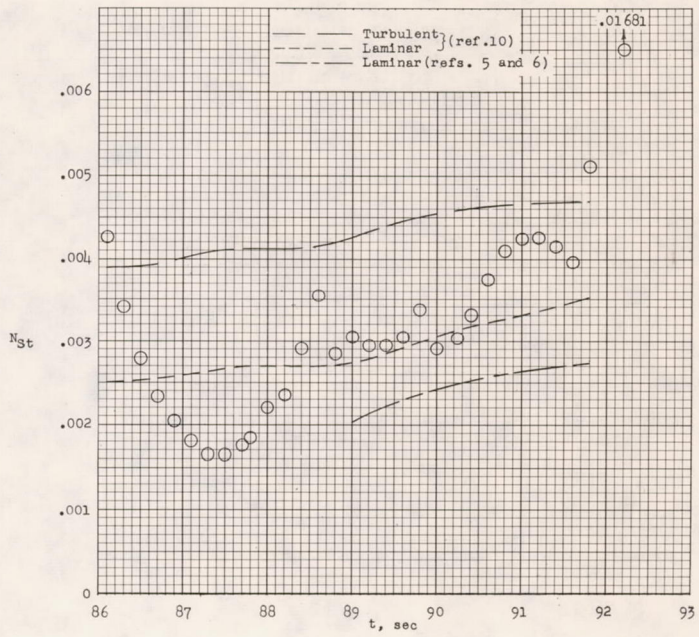


(c) Temperature measuring station 3.

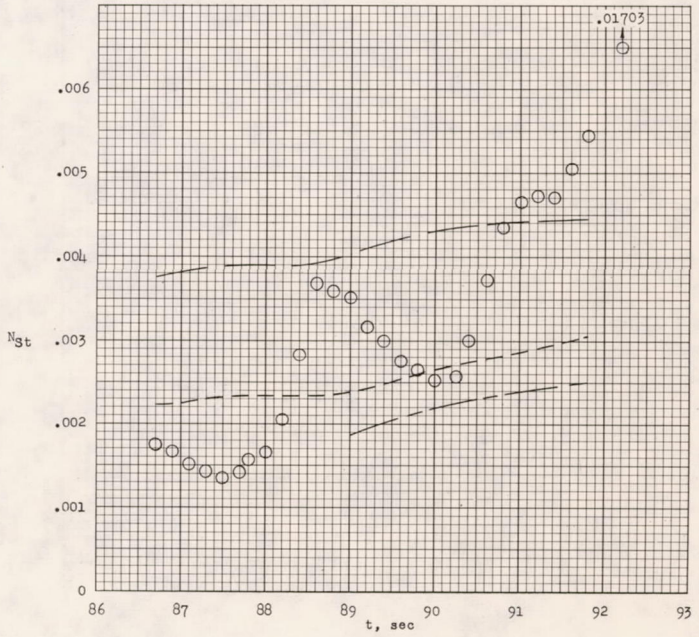


(d) Temperature measuring station 4.

Figure 17.- Continued.

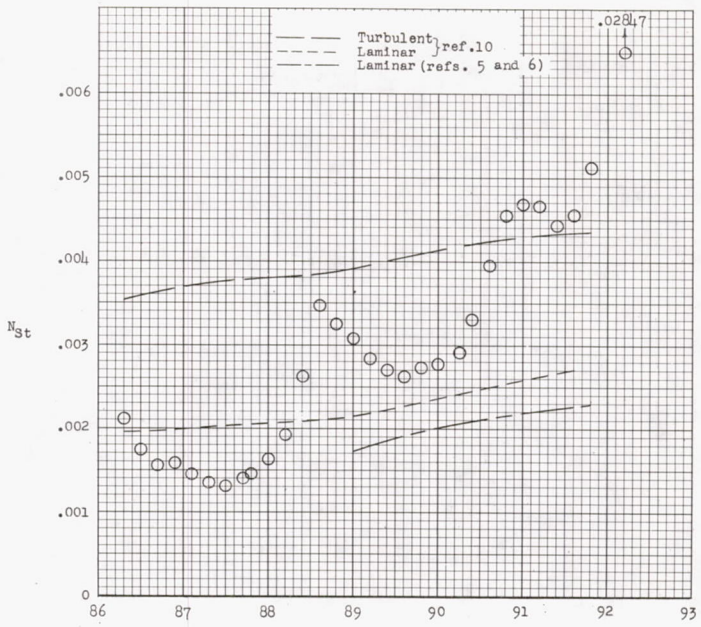


(e) Temperature measuring station 5.

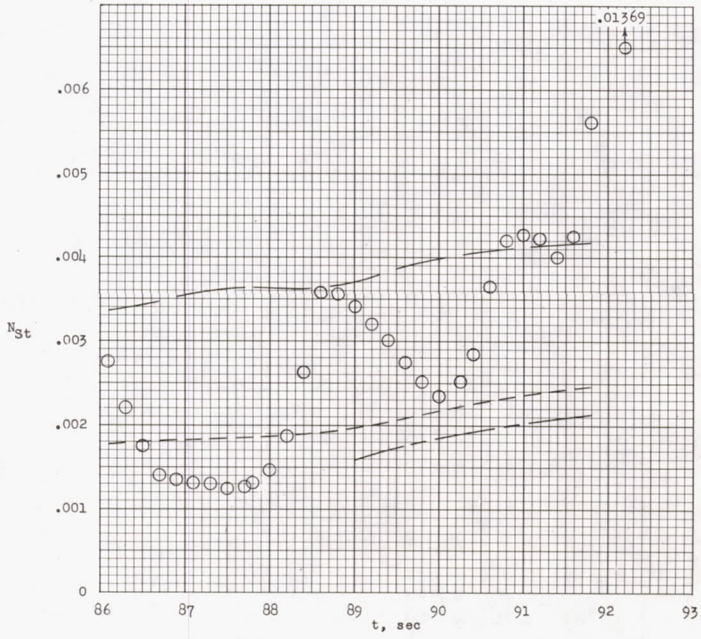


(f) Temperature measuring station 6.

Figure 17.- Concluded.



NACA - Langley Field, Va.